AN APPROACH TO WATERFLOOD OPTIMIZATION: CASE STUDY

A thesis presented to the Department of Petroleum Engineering

African University of Science and Technology, Abuja

In partial fulfilment of the requirements for the award

MASTER OF SCIENCE IN PETROLEUM ENGINEERING

By

OGBEIWI PRECIOUS

Supervised by

Professor Emeritus David Ogbe

African University of Science and Technology

www.aust.edu.ng

P.M.B 681, Garki, Abuja F.C.T,

Nigeria.

July 2016

AN APPROACH TO WATERFLOOD OPTIMIZATION: CASE STUDY

BY

Ogbeiwi Precious

A THESIS APPROVED BY THE PETROLEUM ENGINEERING DEPARTMENT

RECOMMENDED:

…….

Professor Emeritus David Ogbe (Committee Chair)

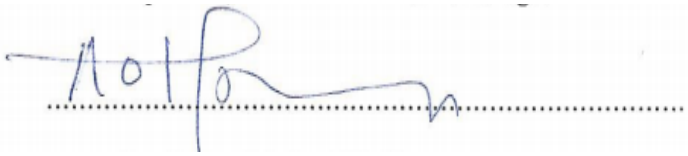

Dr. Alpheus Igbokoyi (Ph.D) (Committee Member)

……

Dr. Mukthar Abdulkadir (Ph.D) (Committee Member)

APPROVED:

…..……

Head of Petroleum Engineering Department

…….

Chief Academic Officer

……...

Date

ABSTRACT

Waterflooding is the most dominant secondary oil recovery method and its popularity is mainly due to the general availability of water, the relative ease of injecting water, the ability of water to spread easily through an oil-bearing formation and the efficiency of water in displacing oil. However, waterflooding is not without its challenges. Factors such as reservoir heterogeneity, lateral and vertical variations in permeability and presence of discontinuities greatly affect this process.

This study is aimed at optimizing waterflooding in a case study using geostatistical reservoir characterization and simulation techniques. The impact of variations in kV/kH ratios across the reservoir on the performance of waterflooding is analyzed. The analysis of the effects of zones of production and injection as well as the waterflood pattern selected on cumulative recovery from a waterflooded reservoir was carried out. The waterflood patterns considered were the regular five-spot, the direct line drive and the staggered line drive patterns. The results were analyzed by evaluating trends of average reservoir pressure, oil producing rate, cumulative oil production and field water-cut over time for several scenarios of the waterflood. These trends were also compared to a base case; a case of reservoir depletion without waterflooding.

The results showed that variations in kV/kH ratio play a significant role in the performance of waterflooding. Finally, the optimal waterflood pattern of all the patterns studied was the direct-line waterflood pattern which gave the highest oil recovery.

This study has demonstrated that geostatistical reservoir characterization and simulation techniques are good tools for reservoir management. It has also shown that variation in kV/kH ratios, zones of injection and production and the waterflood pattern used to produce the oil affect the performance of a waterflooding process greatly.

Keywords: Waterflooding, optimization, static reservoir models, reservoir simulation, permeability, performance.

ACKNOWLEGDEMENTS

First and foremost, I would like to thank God Almighty for His guidance and protection throughout the period of undertaking this work. The ideas He gave me from time to time when I had challenges were indeed helpful.

Secondly, I express my gratitude to Professor David Ogbe for the immense supervision of this work. Your fruitful effort and time spent on this thesis have gone a long way to add quality to it. I also want to thank Coat Engineering, Inc., USA for donating the SENSOR 6K software used for this research.

Thirdly, I would like to appreciate my parents especially my dad for his financial support throughout this research.

Fourthly, my appreciation goes to my Ghanaian brothers who helped me during the period of this research – **Borsah and Evans**. May your days be plenty and joyful. See you guys at the top!

Also, I thank the AUST community especially Mrs. Yetunde, Obed and all my class mates.

DEDICATION

This thesis is dedicated to God Almighty for his love, to my mum, Philomena for her support, and to Mrs. Stella Ekawu whose timely information brought me here.

TABLE OF CONTENTS

LIST OF FIGURES

LIST OF TABLES

CHAPTER 1

INTRODUCTION

1.1 Study Background

To meet the ever-increasing demand for petroleum worldwide, it has become increasingly necessary to produce oil and gas fields more economically and efficiently. Since a significant number of prominent oil fields are mature fields and the number of new discoveries per year is decreasing, it has become more imperative to use secondary oil recovery processes (Nwaozo, 2006).

Waterflooding is one of the most widely used secondary oil recovery means after the exhaustion of the primary depletion energy of a reservoir and it is said to be responsible for high oil production rates in mature oil fields in the U.S and Canada (Craig, 1971). It basically involves pumping water through an injection well into the reservoir. The water then forces itself through the pore spaces and sweeps the oil towards another set of wells known as producers. As a result, there is an increment in the total oil production from the reservoir. However, the percentage of water in the produced fluids steadily increases. On average, this process can lead to the recovery of about one-third of the original oil in place (OOIP), leaving behind about two-thirds (Meshioye et al., 2010). Other secondary recovery methods include CO_2 flooding and hydrocarbon gas injection. These other processes require a nearby source of the inexpensive gas in sufficient volume.

It is commonly said that the high level of production rate and reserves around the world today is as a result of the popularity of water injection (Asadollahi, 2012). The popularity of water injection is mainly due to the following reasons:

- The relative ease of injecting water.
- The general availability of water.

- The ability of water to spread easily through an oil-bearing formation.
- The efficiency of water in displacing oil.

At some point during waterflooding operations, it becomes uneconomical to continue such operations because the cost of removing and disposing water exceeds the net income generated from the oil production, thus the waterflooding has to be stopped. Some wells are still considered economical even at a watercut of up to 99% (Arenas et. al, 2003).

In spite of its popularity, waterflooding is not without its problems. According to Handyside et al. (1992), two common problems generally plague waterflooding. Waterflooding has poor sweep efficiency and a low contact factor. The contact factor is determined by improper displacement in a direction orthogonal to the reservoir strata. In reservoirs with lateral heterogeneity or those in which bedding planes exhibit anisotropy, poor areal displacement efficiency is commonly encountered. That means large areas are left with high oil saturation for a given economically acceptable watercut in the production wells.

In reservoir systems, reservoir internal structure, reservoir rock properties and fluid properties adversely affect production and injection schemes (Kooli, 2010).

1.2 Statement of Problem

Globally, large amounts of hydrocarbon volumes are found in reservoir systems associated with high shale volumes. These shales create discontinuities within the reservoir units. The presence of flow barriers caused by these shales and variations in directional permeability across the reservoir strongly affect the drainage patterns and the sweep efficiency of water injection processes (Awejori, 2014).

Therefore, to accurately estimate the efficiency of a waterflooding process, an assessment of the impact of sand discontinuities or connectivities in these reservoirs is required for realistic performance predictions of the schemes and estimation of associated confidence limits. This is particularly important during the pre-developmental stage when major investment decisions are to be made on the basis of a limited number of exploration wells (Handyside, 1992).

Also, since these reservoir systems are composed of various genetic reservoir units ranging from clean channel lag and storey axis sands with a high net-to-gross to thin-bedded levee over-bank deposits containing lower sand fractions, the selection of reservoir zones for completion of producers and injectors is of key interest to reservoir engineers (Brouwer, 2001).

1.3 Objectives of this Study

The objectives of this study include:

- Investigation on the impact of directional permeability variations across the reservoir and the presence of flow barriers due to shale presence on the waterflood injection patterns, drainage and performance in turbidite reservoirs.
- Investigation on the impact of multizonal completions for production and injection on the efficiency of waterflooding.
- Selection of the optimal waterflooding pattern for oil production using a case study by evaluating the performance of different waterflood patterns.

1.4 Scope of this Work

This research involved the use of a case study in evaluating several waterflood optimizations scenarios. The scope of this research does not include creating an actual optimized development and production strategy that can be implemented in the field of interest. Rather, it involves using the properties of the formation to carry out comparative analysis on several factors that influence waterflood optimization in any given reservoir, such as kV/kH ratios and zones of injection and production (ZoIP). However, the methodology presented and discussed by this research can be applied in carrying out a field-wide development of the area of study.

1.5 Structure of the Report

This report consists of five main (5) chapters.

Chapter one contains the introduction, statement of the problem, objectives, the scope of the work and the structure of the report. This chapter provides a summary of the various methods adopted in carrying out and organizing this research, as well as the process of preparing this project report.

Chapter two provides review of all necessary literature regarding this research. Key concepts regarding the research topic are explained therein. The chapter also gives brief explanations of recent methods adopted by some researchers on waterflood optimization.

Chapter three presents a brief description of the area of study and the method adopted in the study. The simulation processes and some of the software used are also discussed in this chapter.

Chapter four contains the results obtained and its analyses in achieving the objectives of the study.

Chapter five presents the conclusions and recommendations that were drawn from the various analyses.

CHAPTER 2

LITERATURE REVIEW

2.1 Overview of Oil and Gas Recovery

Generally, oil and gas resources are found in underground storages which are made up of porous permeable rocks called reservoirs. These accumulations of hydrocarbons occur in underground traps formed by geological structures. A reservoir is that portion of a trap which contains oil and/or gas as a single hydraulically connected system (Asadollahi, 2012). Most of these hydrocarbon reservoirs can also be hydraulically connected to some volumes of water-bearing rocks called aquifers.

In the reservoir, hydrocarbon fluids can exist as either single phase or two phase state under initial conditions. The single phase may be a liquid phase in which all the gas present is dissolved in the oil. In the two-phase state, the liquid phase called the oil zone, exists under the gas phase which exists as the gas cap. Figure 2.1 shows a typical oil reservoir with the gas cap and underlying aquifer.

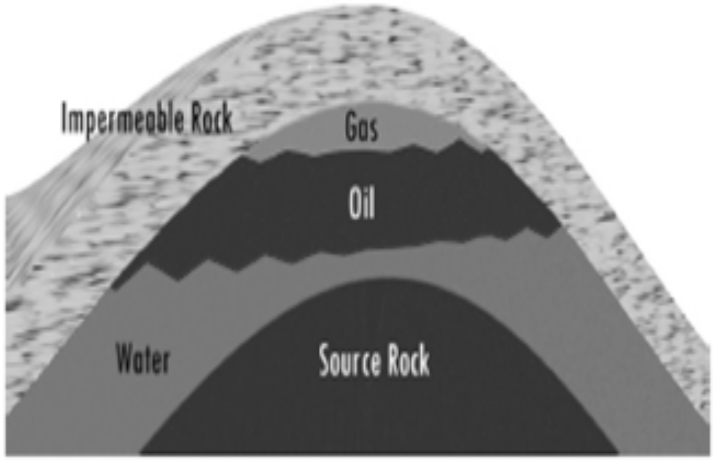

Figure 2.1: A typical underground oil reservoir, Asadollahi, 2012.

Initial production of oil from a reservoir usually involves the use of the reservoir's natural energy. This may involve the use of various mechanisms such as water (aquifer) drive, rock and

fluid expansion, solution gas drive, gas cap drive and gravity drainage in which one or more mechanisms may be predominant. During the production within the reservoir, this predominance may shift from one mechanism to another, either naturally or because of some engineering operations (Asadollahi, 2012).

Most times, the use of the natural driving mechanism is a relatively inefficient process and results in a low overall oil recovery. As a result, it is now a common practice to introduce some form of artificial drive in order to supplement the natural reservoir energy. The most common methods are the injection of gas or water, a process termed secondary oil recovery.

Secondary recovery, is the recovery of oil and/or gas involving the introduction of artificial energy into the reservoir via one wellbore, and production of oil and/or gas from another (Ahmed, 2006). Usually, the selected secondary recovery process follows the primary recovery but it can also be conducted concurrently with the primary recovery. Conventional secondary recovery processes include waterflooding and pressure maintenance by water/gas injection into an aquifer/gas cap (Asadollahi, 2012).

2.2 Waterflooding

Waterflooding is the most dominant secondary oil recovery method and, currently in the United States, a large portion of the oil production (approximately 50%) is recovered from the reservoirs under waterflooding (Lyons, 1996). According to Nwaozo, (2006) its popularity is due to the general availability of water, the relative ease with which water is injected, and the ability with which water spreads through an oil-bearing formation and water's efficiency in displacing oil. However, waterflooding is not always without its challenges, but there is a still sound basis for waterflood projects.

Ahmed (2006) pointed out that in selecting a suitable candidate reservoir for waterflooding, the following reservoir characteristics must be evaluated:

- Reservoir geometry.
- Fluid properties.
- Reservoir depth.
- Lithology and rock properties.
- Fluid saturations.

- Reservoir uniformity and pay continuity.
- Reservoir primary recovery mechanism(s).

In a waterflooding project, two general types of well locations are common: the peripheral or central flooding, and the pattern flooding. In the central flooding, the injectors are grouped together while in the latter certain patterns are repeated throughout the field. According to Asadollahi (2012), the relative location of injectors and producers depends on the type and geology of the reservoir, the volume of reservoir swept by the water, and economics.

In peripheral flooding, the injectors are located around the periphery of the reservoir so that the flood progresses toward the center as shown in Figure 2.2. After sometime, the first rows of producers flood out and are usually converted to injectors. This type of flood can lead to maximum oil recovery with a minimum of produced injectant, and less injectant is required for a given amount of production, but a peripheral flood usually takes longer time than a pattern flood (Lyons, 1996).

Central flooding is the opposite of peripheral flooding in which injectors are placed at the center of the field, and the flood progresses outward.

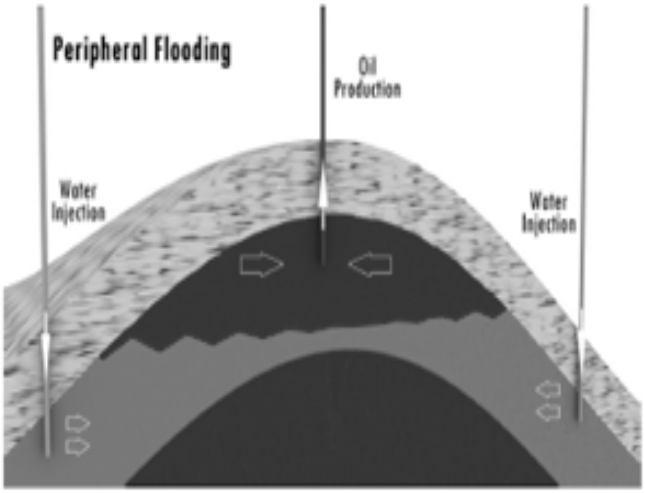

Figure 2.2: Peripheral waterflooding, Asadollahi, 2012.

In pattern flooding, the injectors are positioned among the producers in some repeating fashion. Examples of some common pattern floods are shown in Figure 2.3 below. Pattern flooding is very common, and the selection of the type of pattern depends on the circumstances in a given field.

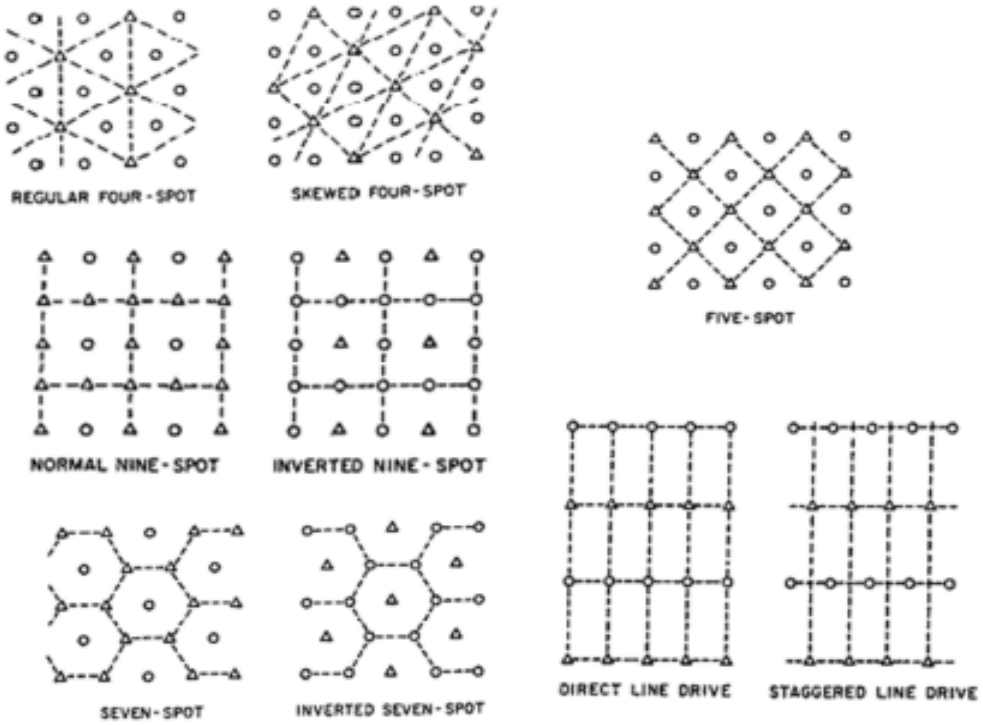

Figure 2.3: Various types of regular waterflood patterns Ahmed, 2006.

2.3 Reservoir Characterization and Simulation

2.3.1 Overview of Reservoir Characterization

Reservoir characterization is the process of incorporating data of different qualities and quantities in such a way that allows one to describe reservoir properties of interest at inter-well locations (Odai et al, 2010). Reservoir characterization helps in generating a more representative geologic model of the reservoir properties. It also enables a better understanding of the reservoir connectivity in static and dynamic conditions by allowing integration of data from different sources (Mondal, 2010).

It has been observed that the success of any hydrocarbon exploration and exploitation program largely depends on the building of a reliable reservoir model. A reservoir's commercial life usually begins with exploration that leads to discovery, followed by characterization of the reservoir.

2.3.2 Overview of Reservoir Simulation

Reservoir simulation is one of the most powerful techniques available to the reservoir engineer (Koederitz, 2004). It plays a very important role in the modern reservoir management process and is used to develop a reservoir management plan and to monitor and evaluate reservoir performance.

The simulation process consists of describing the reservoir (i.e. model construction), matching historical performance, and predicting the future performance of the reservoir under a variety of scenarios.

2.4 Optimization of Oil and Gas Production

Production/reservoir optimization is performed using reservoir models to simulate, predict and optimize the production performance to maximize asset value (Asadohalli, 2012). Over the years, there has been an increasing need for production optimization of reservoir fields due to the global increase in demand for oil and gas. As a result, several applications of optimization algorithms have been developed and these optimization techniques have proved to be beneficial in the various problems of reservoir development, well testing and gas resource distribution (Nwaozo, 2006).

The proceeding section will review the various optimization problems that have been investigated by researchers and their methodologies to solving the existing waterflood problems.

2.4.1 Overview of some methodologies for waterflood optimization

Asheim (1988) studied the optimal control in waterflood reservoirs using reservoir simulation models. He developed a method for numerical optimization of the net present value of an aquifer

drive and artificial water drive by injection. His method used a two-phase reservoir simulator to calculate the net present value (NPV) of a waterflooding scheme in which the control variables were the well rates. The waterflooding scheme that maximized the net present value was numerically obtained by combining reservoir simulation with control theory practices of implicit differentiation. He achieved improved sweep efficiency and delayed water breakthrough by dynamically controlling well flow rates. His results gave an improvement in the net present value of up to 11%.

Spath et al. (1997) studied waterflood optimization using a combined geostatistical 3D streamline approach. They used a combination of stochastic reservoir description techniques and streamline simulation to optimize volumetric sweep efficiency in a mature West Texas waterflood and used an IMPES, finite-difference scheme to validate the results obtained.

Geostatistical techniques including kriging and co-kriging were used to generate realizations of property distributions used, and performance predictions were made for the placement of new infill wells (vertical and horizontal), as well as for pattern modification by selectively shutting in existing injectors. Data from various sources (production, core, log, pressure transient, geological and 3D seismic data) were combined to estimate reservoir properties and to place constraints when distributing permeability, porosity, and net-to-gross thickness.

Their results showed that the combination of multiple realization property distribution with an efficient streamlined model is a much better alternative to the traditional, finite-difference approach.

Brouwer et al. (2001) studied the static optimization of waterflooding for two horizontal smart wells which contained permanent downhole well control valves and measurement equipment. The flow rates of the inflow control valves were kept constant during the waterflooding process until the water arrived at the producer, hence the term “static optimization”. Algorithms were employed to minimize the impact of high-permeability streaks on the waterflood performance by controlling injection and production rates. Their results showed that the optimal rate allocation

can be obtained by controlling the distribution of water arrival times at various segments of the producer.

Nwaozo Jude (2006) studied the dynamic optimization of a waterflood reservoir. His research presented a methodology for optimizing net present value from a waterflood reservoir by controlling the bottom-hole pressures of the production wells with the use of smart well technology. The optimization procedure involved maximizing the cumulative oil production from a waterflood reservoir by adjusting production flow rates. The production wells were smart wells with downhole chokes that could be automatically adjusted. The production well completions were also set such that they could automatically shut off when economic limits based on the watercut were reached.

In his approach, he used a variant of the ensemble Kalman filter (EnKF) technique in the optimization process, and the optimization methodology was validated using some heterogeneous 2-D models with a five-spot pattern waterflood scheme carried out using the Eclipse 100 blackoil simulator. The solution to the optimization problem was the pressure profile of the production well that gave the maximum NPV. The results of the optimization methodology indicated an increase in NPV of up to 9% and an increase in cumulative production of up to 12% of the base case when the geology was known.

Meshioye et al (2010) carried out a research that presented an optimization methodology in which waterflooding was controlled by smart injector well technology to increase NPV. The optimization procedure was performed on three different scenarios of a commingled reservoir having different layer characteristics and it involved a vertical smart injector well, and a production well penetrating fully through the commingled reservoir. An optimization procedure was applied where the rate allocation method was used in each zone of the smart injector well.

The optimization process used smart well technology on the vertical injector and producers to isolate the reservoir into different segments through inflow control devices and packers. Thus, each segment could be treated separately and also as independent wells. Downhole measurements obtained from the smart wells were used to optimize the reservoir.

In this research, the right rate allocation to each zone that gave the maximum oil recovery or NPV was the answer to the waterflood optimization problem. The smart injector well used had inflow control valves (ICVs) that could automatically open and close in order to meet some optimization requirements.
The installation of the smart completion on the injector well resulted in early water breakthrough control and reduction in water recycling in some reservoir layers; which ultimately lead to an increase of 2% - 8% in the NPV.
Ogali (2011) conducted a research which focused on the optimization of waterflood using streamline simulation. The streamline-based simulation workflow used for computing well allocation factors (WAFs) and injection efficiencies was proposed by Thiele et al (2006). These efficiencies were used to optimize oil recovery by effectively reallocating water available for injection. The proposed methodology was validated with a case study which showed that reallocating available injection water to more efficient injection wells in a five-spot pattern waterflood leads to optimization of oil production for each barrel of water injected. From the results, it was also observed that starting injection water reallocation early in the life of the waterflood project optimizes production.
The impact of several factors such as the time to start injection water reallocation, duration of reallocation cycles, zones of injection, kV/kH ratios and formation heterogeneity (using Dysktra-Parsons coefficient) on the performance of waterflooding was also analyzed. The results showed that kV/kH ratio, heterogeneity, and zones of injection all play a significant role in the performance of waterflooding.

2.4.2 This Study Approach

This study is aimed at optimizing a waterflood case study using geostatistical reservoir characterization and simulation techniques. The geostatistical technique, sequential Gaussian co-simulation (co-SGSIM) will be used to generate realizations of reservoir property distributions.

These properties will include: porosity, average permeability and net-to-gross ratio. The distribution of reservoir facies across the reservoir model are also carried out.

Special emphasis is given to data integration from all available sources so as to constrain computed petrophysical values as well as generate fine-scale property distributions within reservoir sequence deposits. The resulting geostatistical models are calibrated to available production data, and used as predictive tools for a waterflood scheme in a simulated model. The forward run will be carried out with the Coates Engineering Sensor 6K reservoir simulator (Coats, 2013).

The impact of variations in directional permeability across the reservoir model were studied by examining different waterflood schemes. The waterflood performance was evaluated by analyzing the trends of field average reservoir pressure, oil producing rate, cumulative oil production and field water-cut over time for several scenarios of the waterflood. These trends were compared to a base case.

A simple optimization methodology involving analyzing the effect of zones of injection and production on a waterflood performance was carried out. The optimization was aimed at increasing the cumulative oil recovery from the reservoir. The optimal zones for injection and production would be those completion zones that give higher oil recovery (and/or pressure support) with considerable water-cut.

CHAPTER 3

STUDY METHODOLOGY

3.1 Introduction

This research involved the use of a case study in evaluating several waterflood optimization scenarios. The data for the case study was obtained from the Mars N/O field in the Gulf of Mexico, USA. Since the reservoir was very large with estimated reserves of 534 MMSTB at the discovery, a section of it which was arbitrarily named the T-1 reservoir was studied in this research. The scope of this research does not include creating an actual optimized development and production strategy that can be implemented in this field of interest. Rather, it involves using the properties of this formation to carry out comparative analysis on several factors that influence waterflood optimization in any given reservoir, such as kV/kH ratios and zones of injection (ZoI).

A simple optimization methodology involving analyzing the effect of zones of injection and production on cumulative oil recovery was carried out. The optimization results were then applied to analyze the optimum waterflood pattern for developing the field using reservoir simulation techniques. Tools used in this research include Stanford Geostatistical Modeling Software (SGEMS) and Coats Engineering Sensor 6K (Coates, 2013). SGEMS was used to populate the reservoir model with petrophysical properties, such as net-to-gross ratio, shale

volume, porosity, and permeability. Sensor 6K was used in carrying out simulations for the different scenarios analyzed.

3.2 Case Study: The T-1 Reservoir

The data for this study is derived from Lach, 2010. The Mars N/O sands are located in the Gulf of Mexico and are made up of a series of turbidite sands of the Miocene to Pliocene age which is deposited within a minibasin. The Mars N/O reservoir was a good candidate for secondary recovery because the reservoirs have limited aquifer influx, are very over-pressured and compacting, and under-saturated (Lach, 2010). The reservoirs also have good structure relief, good connectivity and directional permeabilities. Its sands are generally characterized as sheet sands and channelized deposits but massive fine and very-fine grained sands are also observed. The sheets have excellent lateral pressure communication and shales at the internal zones do not necessarily divide the reservoir into compartments as seen from production and pressure history.

Seawater injection commenced in 2004 when reservoir pressure was about 6,800 psia, approximately 4,500 psi below the original 11,305 psia. Cumulative injection at June 2009 was 46 MMBBL with significant water break-through occurring. Some of the waterflood objectives are to maintain/stabilize pressure to prevent the sands from producing below their bubble points and to minimize well completion failures (Lach, 2010**)**. Its original oil in place is estimated at 534 MMSTB.

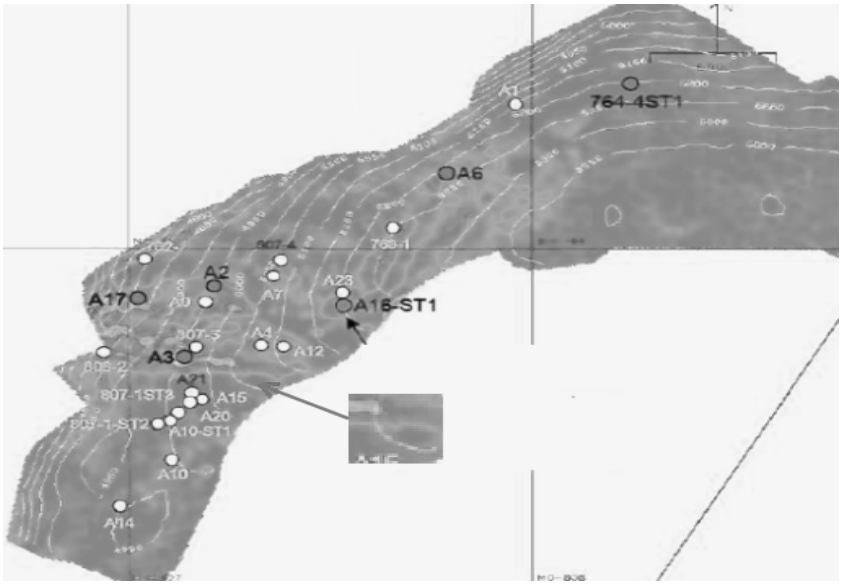

Figure 3.1: Structure map of the Mars oil field showing wells placement and area of interest (T-1 reservoir) (Lach, 2010).

Table 3.1: Average properties of the T-1 reservoir (after Lach, 2010).

PROPERTY	VALUE
Area (Acre)	4917
Average porosity, ø (%)	28
Average Water Saturation, S_{wa} (%)	0.22
Net/gross sand	0.9
Average Permeability, (mD)	125
Reservoir thickness, (ft)	99
Datum depth (ft)	16726
Initial reservoir pressure at datum, P_R (psi)	11305
Bubble point pressure (psia)	6306
Oil viscosity, μ (cP)	0.782
Oil initial FVF (rb/stb)	1.39

3.3 Map Digitization.

The open-source software Plot Digitizer 2.6.4 is a program for digitizing graphs and plots. In this study, it was used to generate coordinates for the available isopach and net-to-gross maps. It was also used to correlate petrophysical data from each well in the T-1 reservoir with their respective coordinate locations.

3.4 Estimation of Petrophysical Parameters of Interest.

The petrophysical parameters of interest were estimated using well established methods which have been known to work perfectly in the Gulf of Mexico area. The petrophysical parameters of interest were those that were to be used in the estimation of the oil in place of the study area. The procedure used for the estimation of these properties is described in the following sections:

3.4.1 Net Pay Thickness (Net/Gross).

This is the ratio of the sum of the thicknesses of the net pay zone to the total thickness or depth of the well (Awejori, 2014). This is usually obtained by measuring from the top of the sand to the bottom of the sand. The net thickness is composed of the aggregation of delineated net pay zones established using some petrophysical logs. From this point, the ratio of the net to gross reservoir thickness can then be estimated for each well.

3.4.2 Shale Volume (V_{sh}).

It is often observed that the zones delineated by a gamma ray log as sand are not actually 100% sand but rather a combination of sand and some amount of shale or clay. The volume of shale (Vsh), in these sand bodies can be estimated by means of the equations given below. Firstly, the gamma ray index, I_{GR} is calculated from the gamma ray log using the formula presented below:

$$I_{GR} = \frac{(GR_{\log} - GR_{min})}{(GR_{max} - GR_{min})} \quad \text{----------}$$

3.1

Where: I_{GR} is the gamma ray index, GR_{log} is the gamma ray log reading of the formation, GR_{min} is the gamma ray for a complete sand matrix zone (clay free zone) and GR_{max} is the gamma ray for a complete shale zone (100% clay zone).

The shale volume is then determined using the gamma ray index obtained above, and below using the Larionov equation for calculating volume of shale for unconsolidated tertiary sandstones (Tiab, 2015).

$$V_{sh} = 0.083 * \left[2^{(3.7 \times I_{GR})} - 1\right] \quad \text{---------- 3.2}$$

3.5 Reservoir Characterization and Modelling

3.5.1 Data Analysis

Stanford Geostatistical Modeling Software (SGEMS), an open-source computer package for solving problems involving spatially related variables was used (Remy, 2004). Each reservoir property data was assessed using histograms and variograms. For each property, anisotropic variograms were used to adequately capture the spatial correlation between data points. The properties evaluated include: total porosity, absolute permeabilities and net-to-gross ratio.

Facies modelling

Literature has shown that there are many methods for building facies models (Chang, 2010). These methods can be used to:

- Measure and define facies and facies models.
- Transfer geological information into digital data to quantify geological facies and facies models.

The numerical data based on geological facies models can then be upscaled and used in reservoir simulations. These methods include subsurface facies analysis methods; geostatistics and stochastic simulation methods, and so on (Chang, 2010).

Subsurface methods apply subsurface information, including geological methods (well logs and cores), and geophysical methods (Chang, 2010). Since almost every well is designed to use well log instruments to measure subsurface rock physical properties such as resistivity, sonic velocity and density, log data becomes the most popular, frequently used information for subsurface studies such as subsurface mapping, correlation, and facies analysis.

Among logging methods, the most useful information for geological analysis comes from spontaneous potential (SP) logs and gamma-ray (GR) logs (Cant, 1992). These two types of logs are always applied to correlate subsurface lithologies and to describe lateral facies distribution through curve shape analysis, subsurface mapping, and subsurface facies analysis.

Apart from geological methods, geostatistics, and stochastic modeling are very useful in quantifying geological facies models' data. These methods include stochastic and geostatistics modeling (including variogram-based geostatistics modeling, object-based stochastic modeling, multiple-point geostatistics modeling), and deterministic modeling. For this research, an integration of the geological method (the gamma-ray log) and geostatistics method (variogram-based modeling) will be considered in modeling facies.

The T-1 reservoir is an offshore Gulf of Mexico reservoir consisting of deepwater turbidite sands and shale. The four facies of interest are (4) clean turbidite sandstone with a minor fraction of concretions, (3) sandstone with a significant proportion of concretions, (2) sandstone with significant concretions mixed with shale, and (1) clearly non-reservoir facies consisting of shale and entirely cemented sandstone. The spatial distribution of these facies types has an overwhelming effect on fluid flow. A reservoir characterization study was undertaken to model the facies distribution. The final facies models were used for reservoir management decision making. The following codes were used to represent the respective facies. These codes can be obtained from the well logs a sample of which is shown in Figure 3.2:

Table 3.2: Lithofacies and their corresponding codes

Facies	Codes
Clean sandstone	4
Fairly shaly sandstone/ fines	3
Very shaly sandstone	2
Shale/clay	1

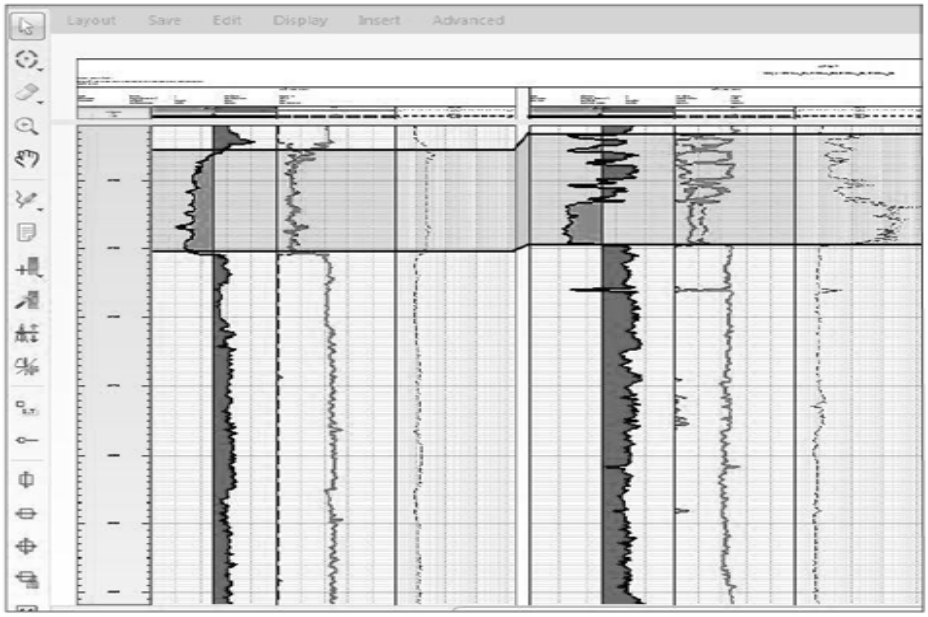

Figure 3.2: Typical log for wells in a turbiditic reservoir (Awejori, 2013)

From the histogram plot (Figure 3.3a), a unimodal distribution was observed with shale (facies 1), being the most common lithofacies in the T-1 reservoir. Also evident is the reservoir zone of interest containing some significant amount of sand (facies 4). To model the spatial correlation between the data points, anisotropic variograms were used in the variogram analysis as shown in Figures 3.3(a) and 3.3(b). This model was then used in the realization generation.

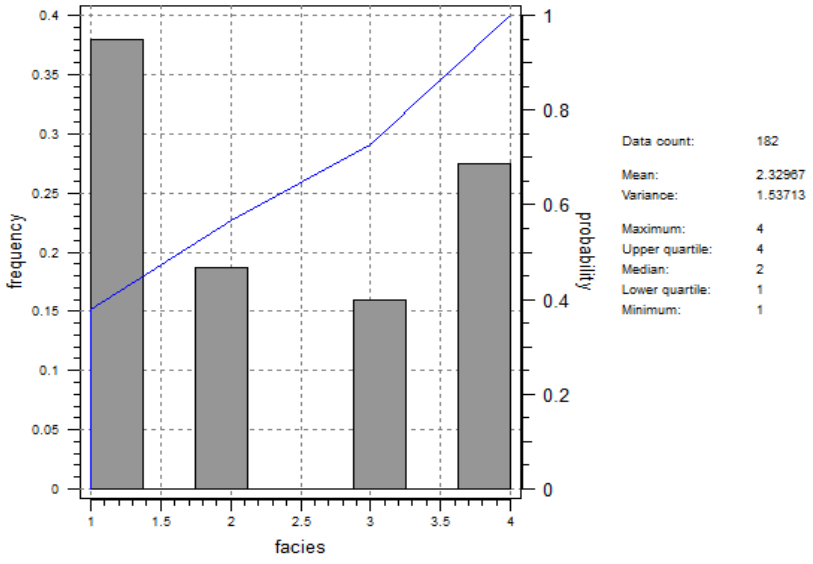

Figure 3.3(a): Histogram for facies

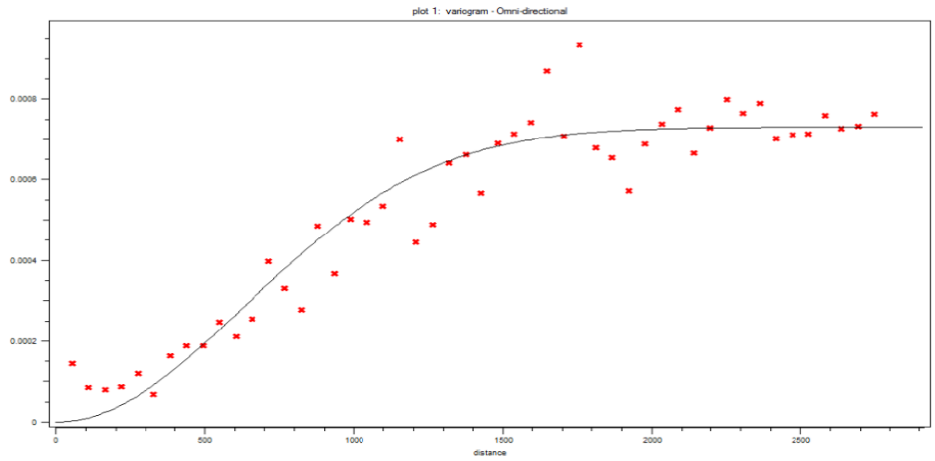

Figure 3.3(b): Variogram for facies.

Figure 3.3: Histogram and Variogram Analysis for facies.

In order to adequately distribute petrophysical properties within the reservoir model, it necessary to model these properties for each of the facies observed in the reservoir. These properties included permeability, porosity and shale volume. The variograms generated are shown in Appendix A1.

Total Porosity

From the histogram for porosity shown in Figure 3.4(a), a unimodal porosity distribution is observed with the minimum and maximum porosity values of 0.07 (6.96%) and 0.385 (38.5%) respectively. The most occurring porosity values are between 0.25 and 0.26. The mean porosity value is 0.24 (24.3%) and the standard deviation is 0.06 (6.5%). This means that a significant proportion of the reservoir contain sands ranging from clean sandstone to sandstone of low shale content, with good porosities.

To aid in the generation of equiprobable realizations, variogram analysis was conducted on the porosity data set and the Gaussian model was also used to fit the data set by visual inspection, and variogram directions captured the spatial variation in the porosity data points. Figure 3.4(b) shows the anisotropic variograms generated.

Due to the sparseness of the data points used in the model, it was necessary to generate cross variograms for porosity as the primary variable and shale volume, V_{sh} as the secondary variable. Figure 3.4(c) shows the cross variogram generated. The shale volume was generated for the individual wells in the T-1 using methods described in section 3.2.2. The anisotropic and cross variograms generated were then used in the building of equiprobable realizations of the porosity for the model.

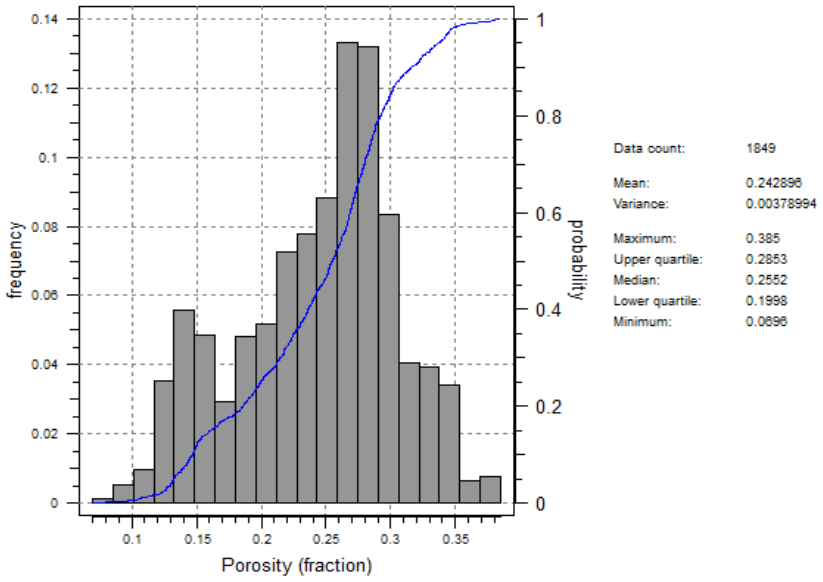

(a) Histogram for porosity data

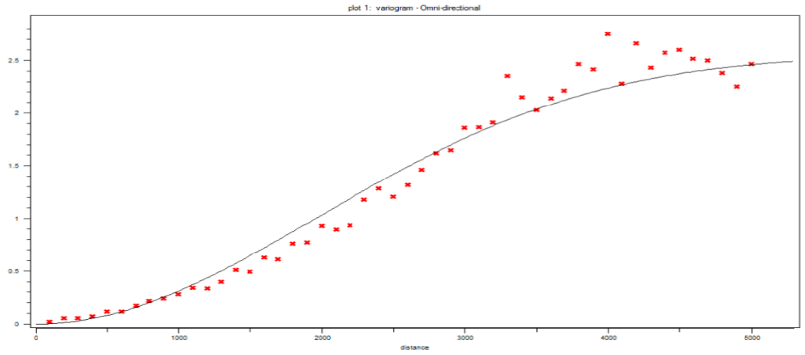

(b)Anisotropic variogram for porosity

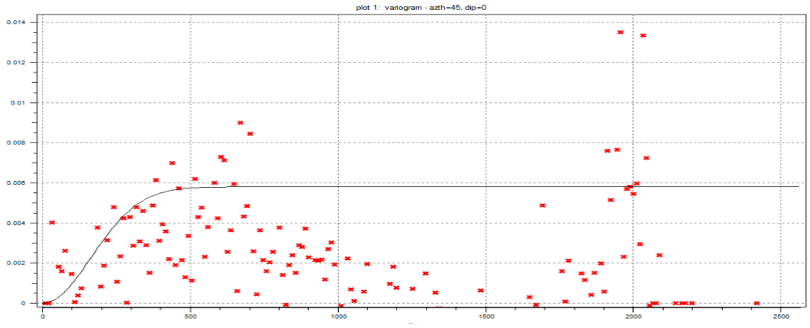

(c) Cross variogram for porosity and shale volume.

Figure 3.4: Histogram and Variogram Analysis for Porosity.

Permeability

When considering total permeability, the values of K ranged from as low as 0.0001md to 1032md, and the majority of the values being between 10-100md. The type of variogram that would have been used to characterize this sample would have been rarely useful because the values would have been clustered at one end.

One way of overcoming this challenge was to transform the sample data in some way so that some sample characteristics are evident from the histogram plot using the log transform. From the research analysis, the log k distribution was more symmetric than the permeability distribution.

From the histogram plot of the permeability data, a unimodal didtribution was observed as shown in Figure 3.5(a). The range 10-100md (logperm values of 1-2) was observed to be the most likely. These values correspond to the porosity values observed in Figure 3.4(a), validating the fact that the reservoir model contains significant proportions of sand. The average permeability is 1.92 (83.1 md) and the standard deviation is 1.87 (73.79 md). The range of log perm values was between -4.05 (0.0001md) and 3.43 (2700 md).

A variogram was then built to capture the spatial variation of permeability between data points. This variogram in combination with the anisotropic variogram earlier generated for porosity was then used in the building of equiprobable realizations of the permeability distribution across the model using a sequential Gaussian co-simulation (COSGSIM). This was due to the sparseness of the data points used in the model. Hence, a cross variogram for permeability as the primary variable and porosity as the secondary variable was built. Figure 3.5 (b) shows the anisotropic variogram generated and Figure 3.5 (c) shows the cross variogram generated.

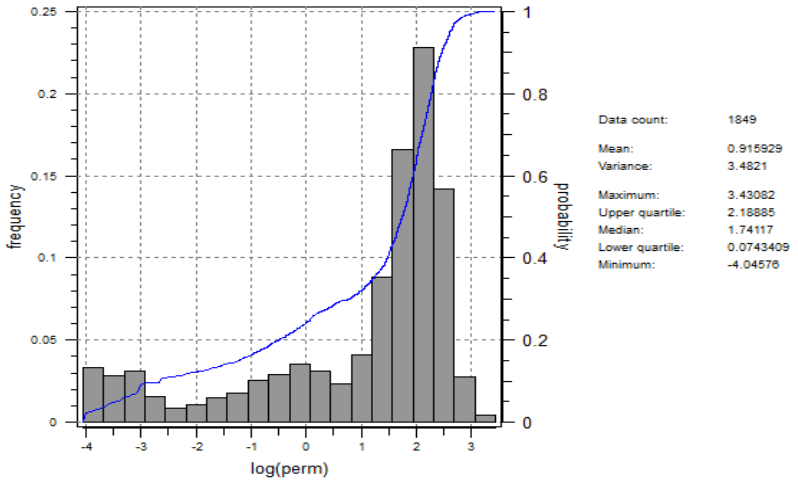

(a) Absolute permeability histogram

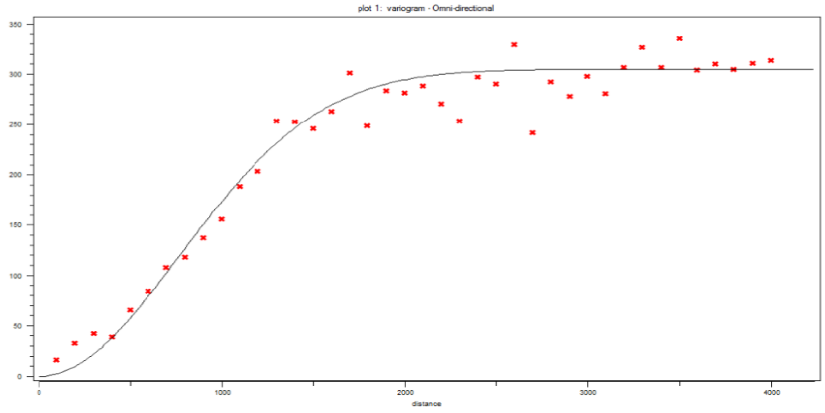

(b) Anisotropic variogram for permeability

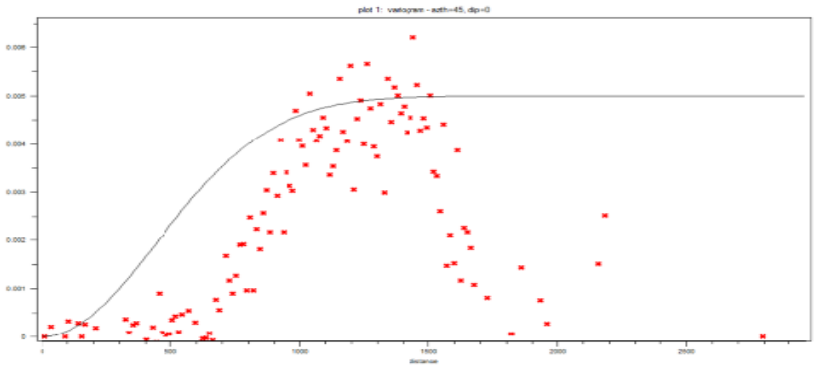

(c) Cross-variogram for permeability and porosity.

Figure 3.5: Histogram and Variogram Analysis for permeability.

Net-To-Gross

As seen from the Figure 3.6(a), the NTG values peaked at 97.4% with the lowest value occurring at 55.4%. From the histogram plot, a unimodal distribution was observed. It was also observed that the most occurring or likely NTG value is around 55%. The mean value is 76.03% while a standard deviation of 19.6% was observed.

To model the spatial correlation between the data points, anisotropic and cross- variograms were used in the variogram analysis as shown in Figures 3.6 (b) and (c). This model was then used in the generation of realizations. Also, it was necessary to generate cross variograms for net-to-gross as the primary variable, and porosity as the secondary variable due to the sparseness of the data points used in the model.

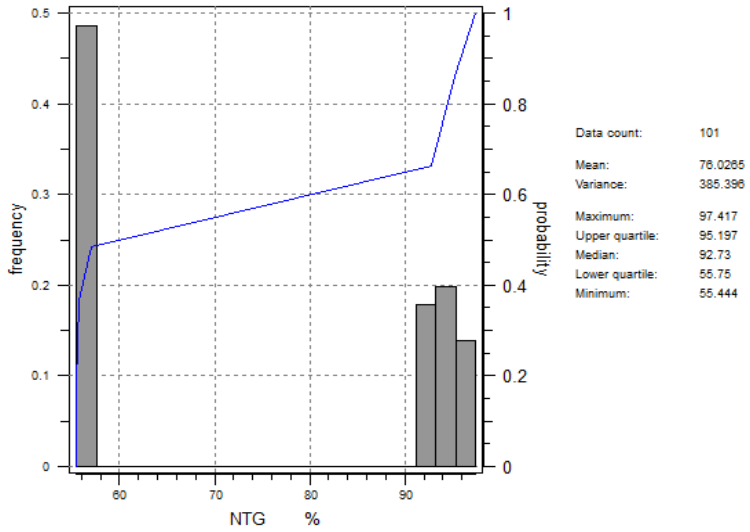

(a) Histogram for net-to-gross

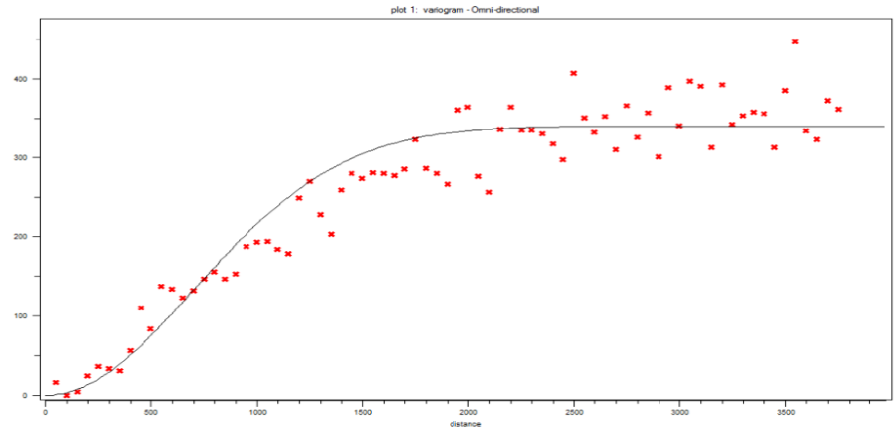

(b) Variogram for net-to-gross.

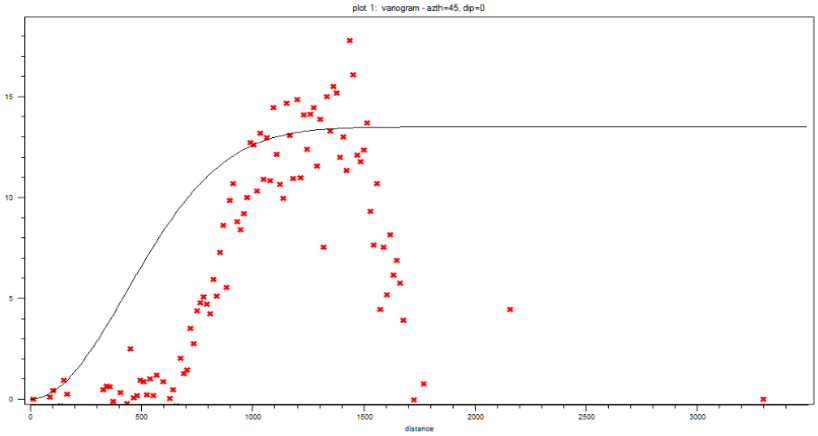

(c) Cross-variogram for net-to-gross and porosity.

Figure 3.6: Histogram and Variogram Analysis for NTG.

Shale volume

As shown in the Figure 3.7(a), a unimodal distribution of shale volume was observed with the minimum and maximum values for NTG at 0 % and 97.3% respectively. It was also observed that the most occurring or likely shale volume value for the wells considered is around 80 - 90% (i.e. the reservoir a significant amount of shale). The mean value is given as 56.02%.

To model the spatial correlation between the data points, an anisotropic variogram was generated as shown in Figure 3.7(b). This model was then used in the realization generation.

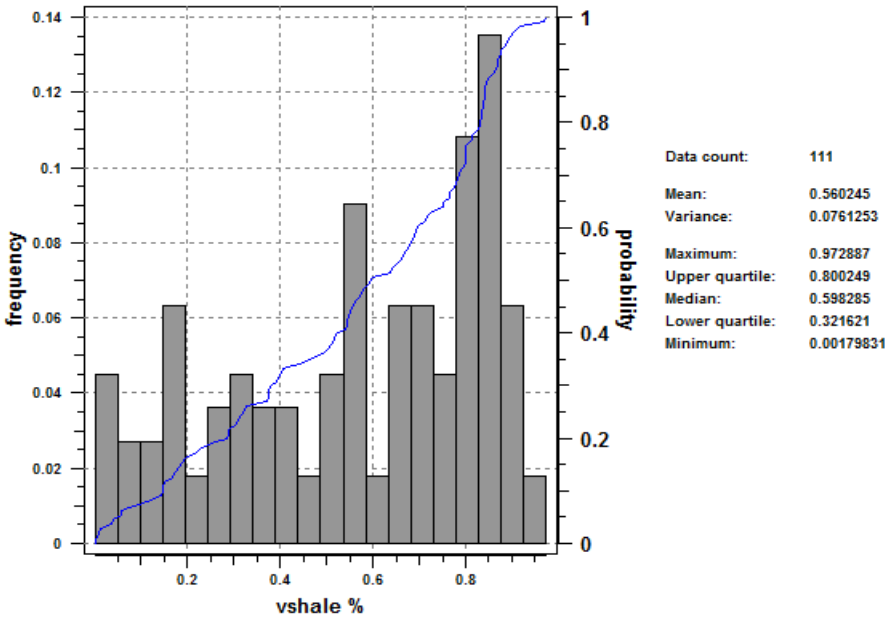

(a) Histogram for shale volume

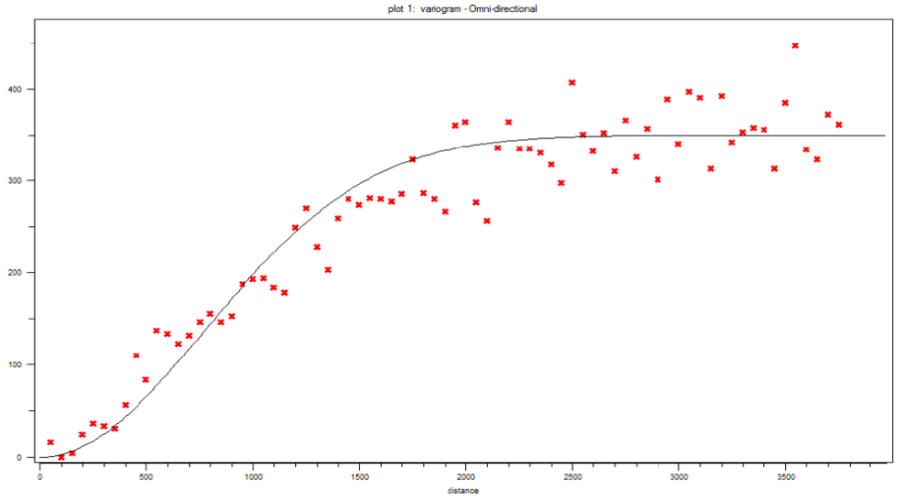

(b) Shale volume variogram

Figure 3.7: Histogram and Variogram Analysis for shale volume.

3.5.2 Building of Reservoir Realizations

To statistically estimate the reservoir properties over the entire volume of the T-1 reservoir model, simulation was used. Stochastic simulation was used instead of kriging to make it possible to generate multiple equiprobable realizations of the reservoir.

Sequential Gaussian Co-Simulation of Porosity, Permeability and NTG

Sequential Gaussian co-simulation (COSGSIM) was used to generate realizations of the reservoir properties accessed. The parameters obtained from the variogram analysis were used in this exercise. For each property, a maximum conditioning data of 12 was used with a seed value of 14071789. Due to the sparseness of data points in the model, it was also necessary to perform co-kriging on some reservoir properties in the model. These properties are porosity and shale volume, permeability and porosity, and finally net-to-gross and porosity.

The sequential Gaussian co-simulation algorithm allows us to simulate a Gaussian variable (such as porosity and permeability) while accounting for the secondary information (such as shale volume), (Remy, 2004).

If $Z_1(u)$ and $Z_2(u)$ are two correlated random variables, where $Z_1(u)$ is the primary variable and $Z_2(u)$ is the secondary variable, the implementation of the primary variable conditioned to both the primary and secondary data is as described below (Remy, 2004):

1. If necessary, transform Z_1 and Z_2 into Gaussian variables Y_1 and Y_2, according to Eq. (3.1) below. It is ensured that the transformed variables Y_1 and Y_2 are at least bi-Gaussian.

$$Y(u)=G^{-1}\left(F\left(Z(u)\right)\right)\ldots\ldots\ldots\ldots\ldots\ldots\ldots\ldots\ldots\ldots\ldots\ldots 3.3$$

2. Simulate variable Y_1:
   a. Define a path visiting each node of the grid.
   b. At each node **u**, the local conditional cumulative distribution function is Gaussian; its mean is estimated by the simple cokriging estimate and its variance by the simple cokriging variance. The conditioning data consists of the original primary and secondary data, and the previously simulated values.
   c. Draw a value from the previous ccdf and add it to the data set.
   d. Proceed to the next node in the path and repeat the two previous steps until all nodes are visited.
3. "Back-transform" the simulated values $y_1,\ldots,y_N$ into $z_1,\ldots,z_N$:

$$z_1=F_1^{-1}\left(G_1\left(y_{i,1}\right)\right)i=1,\ldots,N\ldots\ldots\ldots\ldots\ldots\ldots\ldots\ldots 3.4$$

Where, F_1 is the target distribution function of Z_1 and G_1 is the standard normal cdf.

Sequential Indicator Simulation (SISIM) of Facies

The algorithm SISIM relies on indicator kriging to infer the conditional cumulative distribution functions $F_Z(u_{k+1} \mid (n+k))$, $k = 1, \ldots, N-1$ of the equation below (Remy, 2004):

$$F(\mathbf{u}_1,\ldots,\mathbf{u}_N; z_1,\ldots,z_N \mid (n)) = F(\mathbf{u}_1; z_N \mid (n+N-1))* F(\mathbf{u}_{N-1}; z_{N-1} \mid (n+N-2))* \cdot \cdot \cdot F(\mathbf{u}_2; z_2 \mid (n+1))* F(\mathbf{u}_1; z_1 \mid (n)) \quad \ldots\ldots\ldots 3.5$$

If Z(u) is a continuous variable. SISIM implements the algorithm given below.

1. Choose a discretization of the range D of Z(u): $z_1, \ldots, z_K$
2. Define a path visiting all locations to be simulated
3. For each location u along the path:
   a. Retrieve the neighboring conditioning data of location u: $z(u_\alpha)$, $\alpha = 1, \ldots, N$
   b. Turn each conditioning datum $z(u_\alpha)$ into a vector of indicator values:

$$v(u_\alpha) = [i(z(u_\alpha), z_1), \ldots, i(z(u_\alpha), z_K)].$$

The indicator variable is defined as:

$$i(\mathbf{u}, z_k) = \begin{cases} 1 & \text{if } z(\mathbf{u}) \le z_k \\ 0 & \text{otherwise} \end{cases}$$

   c. Estimate the indicator random variable $I(u, z_k)$ for each of the K cutoffs by solving a kriging system. The simple kriging estimator is given by:

$$\lambda_\alpha(I(u_\alpha, z_k) - ¿ E\{I(u_\alpha, z_k)\}) \quad \ldots\ldots 3.6$$

   d. $$I^*(\mathbf{u}, z_k) - E\{I(\mathbf{u}, z_k)\} = \sum_{\alpha-1}^{N} ¿$$

   e. The estimated values, $i^*(u, z_k) = \text{Prob}^* (Z(u) \le z_k)$, after correction of order-relation problems, define an estimate of the cumulative distribution function $F_{Z(u)}$ of the variable Z(u). Draw a value from that ccdf and assign it as a datum at location **u**.
   f. Loop until all locations are visited.
4. Repeat the previous steps to generate another simulated realization.

3.5.3 Static Modeling

Facies

The Sequential indicator simulation algorithm was used to model the facies distribution within the model. Figure 3.8(a) shows a realization map generated.

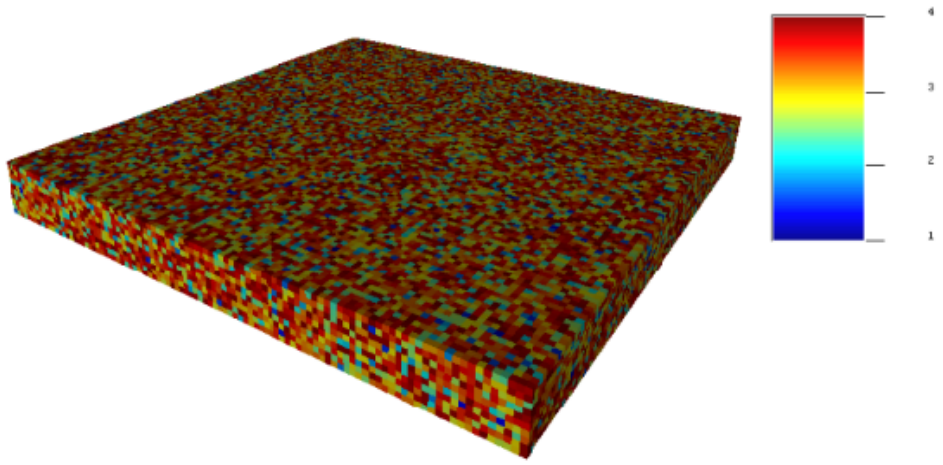

Figure 3.8(a): Facies simulation map across the model.

Also presented below in Figures 3.8 (b) through to 3.8 (d) are simulation maps showing the distribution of facies in layers 1, 3 and 4. Simulation maps for facies distribution in layers 2, 5 and 10 are presented in Appendix B.

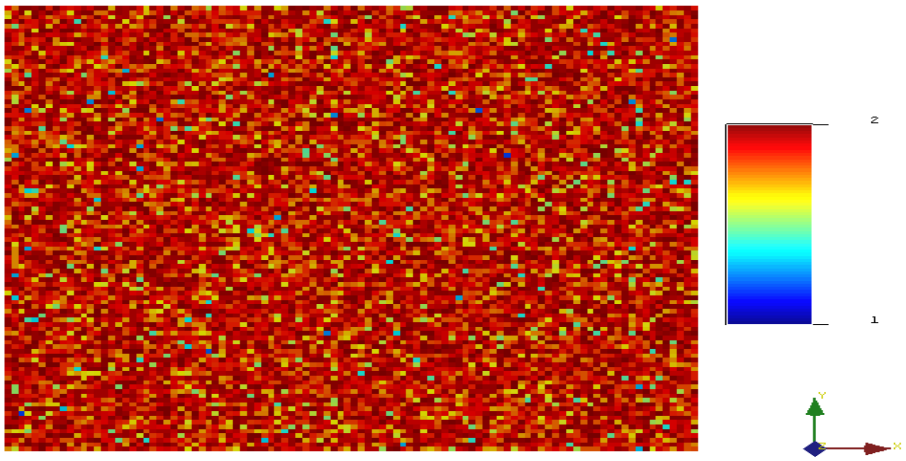

Figure 3.8(b): Simulation map for facies distribution across layer 1.

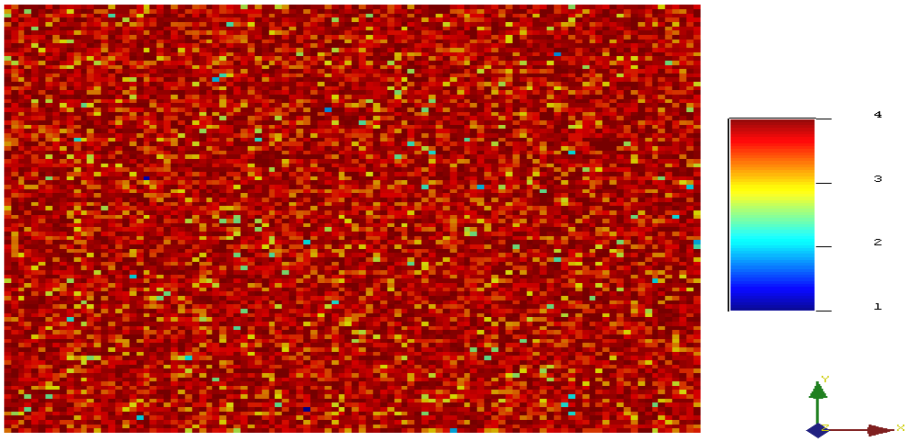

Figure 3.8(c): Simulation map for facies distribution across layer 3.

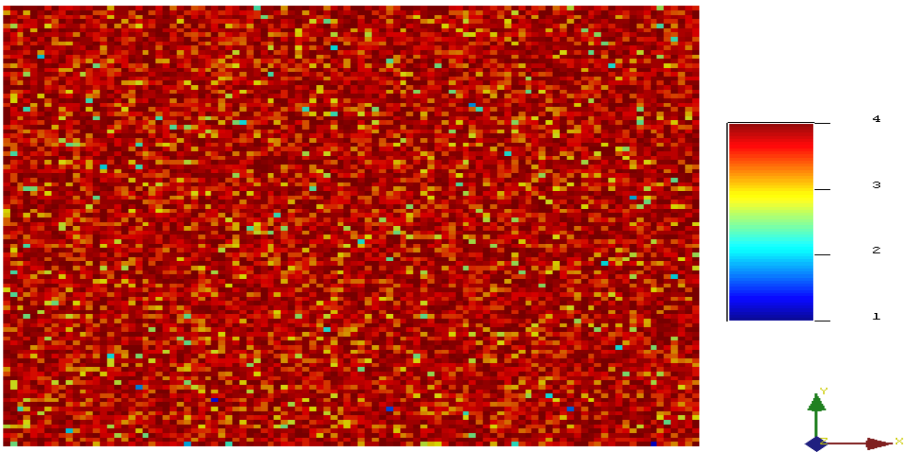

Figure 3.8(d): Simulation map for facies distribution across layer 4.

Figure 3.8: Facies simulation maps.

Porosity

To model porosity, the sequential Gaussian co-simulation algorithm was used to generate a realization map. The sequential Gaussian co-simulation used the mean and variance of the simple kriging in which the trend component is assumed to be constant and the mean is known and grids of simulated values are generated.

Figure 3.9 shows a map generated for different realizations of total porosity across the model.

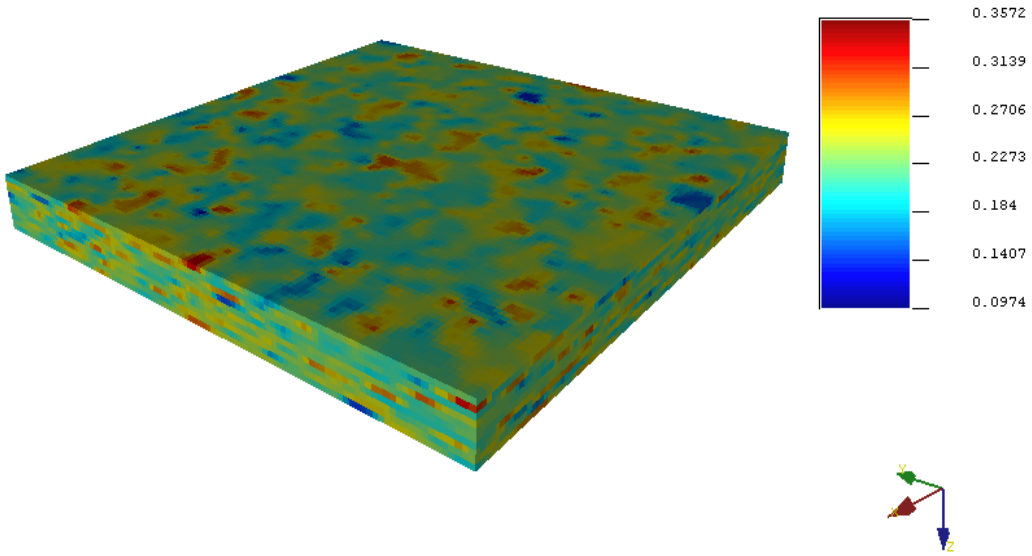

Figure 3.9: Simulation map for total porosity.

From Figure 3.9, it can be seen that the reservoir is characterized by interjections of low-to-high effective porosity values along its depth. This is largely due to the presence of flow barriers as a result of sequential deposition of sand and shale producing sequences of sand and shale. This causes layering in these kinds of systems.

Permeability

The sequential Gaussian co-simulation algorithm was used to model the average permeability in which five realizations of permeability were generated.

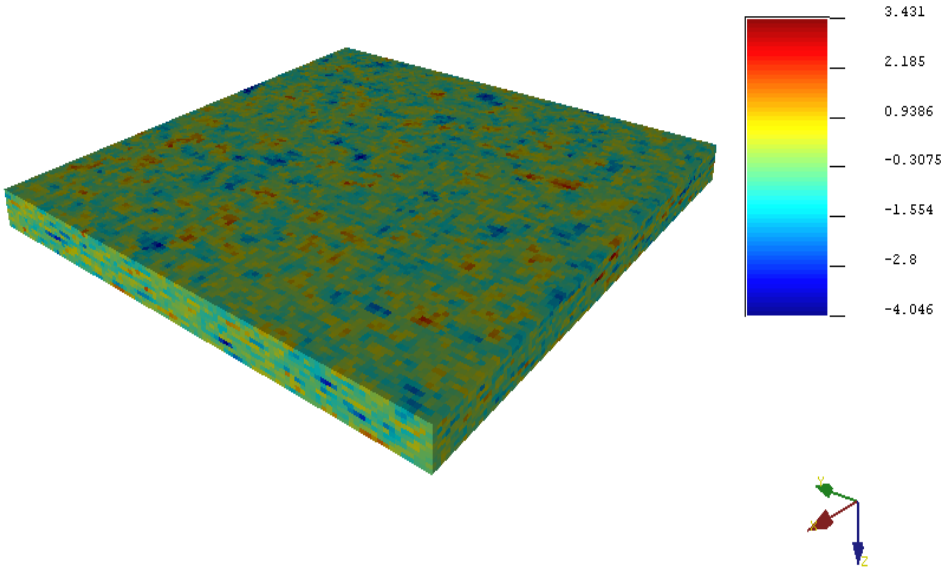

Figure 3.10: Simulation map of permeability.

Figure 3.10 shows a simulation map generated for average permeability in its log transformation. It can be clearly seen that there is variation in the permeability values with increasing reservoir depth. This is a common attribute of reservoir systems.
It should be noted here that, the values obtained from the COSGS simulation are log permeabilities (log k). They must first be converted to actual permeability values by taking the antilogarithm of the values obtained from the simulation, before applying them to the reservoir grid model.

Net-to-Gross

To properly model net-to-gross across the model, the sequential Gaussian co-simulation algorithm was also employed. Figure 4.5 shows the realization map generated.

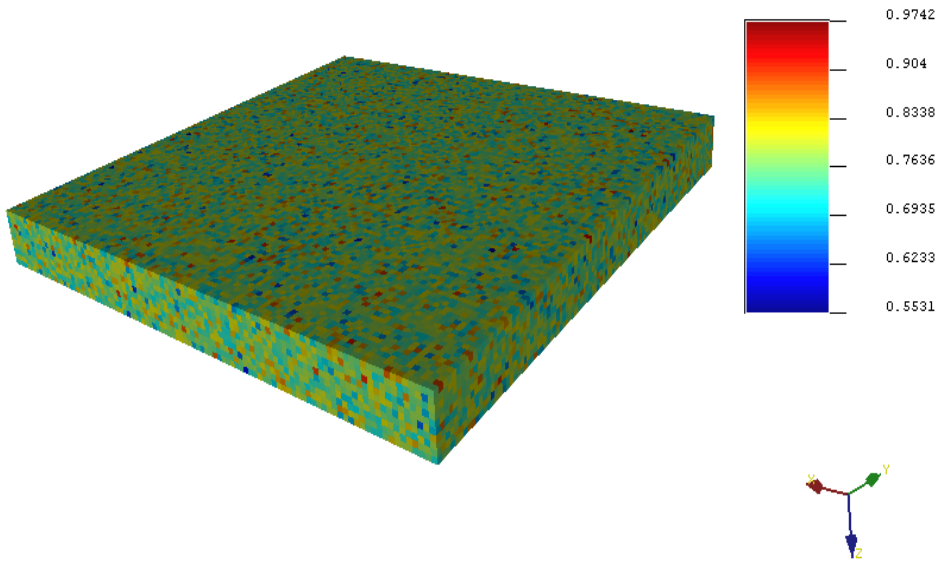

Figure 3.11: NTG simulation map.

Shale Volume (Vsh)

The sequential Gaussian co-simulation algorithm was used to model shale volume across the T-1 model. Figure 3.12 shows the realization map generated.

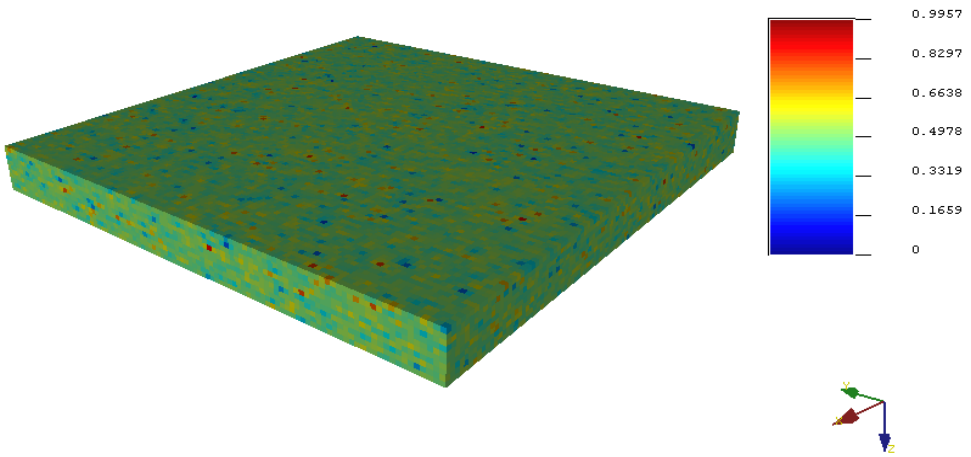

Figure 3.12: V_{sh} simulation map.

3.6 Estimation of Original Oil in Place (OOIP)

3.6.1 Ranking of Static Reservoir Models Built

Five static equiprobable descriptions of each reservoir property were generated using SGEMS. Table 3.3 shows the results of the statistical means obtained from the realizations maps generated for porosity, absolute permeability, and net-to-gross while comparing them with the means of the properties before simulation.

Table 3.3: Summary of the statistical means before and after building realizations

PROPERTY	BEFORE COSGSIM		AFTER COSGSIM		Real. No.
Porosity	Mean	0.24	Minimum mean	0.15	2
			Mean (for all real.)	0.19	
			Maximum mean	0.24	3
Permeability	Mean	1.92 (83.1mD)	Minimum mean	1.86 (65.3 mD)	5
			Mean (for all real.)	1.82 (66.5mD)	
			Maximum mean	1.889 (76.9mD)	3
			Minimum	68.06%	4

Net to Gross	Mean	76.03%	mean		
			Mean (for all real.)	69.11%	
			Maximum mean	71.05%	3

Generally, the mean values after simulation of the petrophysical properties are slightly smaller than those of the raw data. This observation may be as a result of the variogram parameters employed for each property. Also, the variation in the maximum and minimum average values (Table 3.3) suggest the extremely high and low cases of what the reservoir static model could be.

Based on results shown in Table 3.3, OOIP was calculated using the values of the third realization generated with the Sequential Gaussian co-simulation (COSGSIM) for porosity and net-to-gross. Also, the following constant property assumptions were made:

- Water Saturation = 22%
- Formation volume factor, B_o = 1.39 rb/stb
- Average reservoir thickness = 99 ft
- Area of each grid block = 40, 000 ft^2

The original oil in place in stock tank barrel for each gridblock in the map is given by:

$$OOIP = \frac{A \times h \times \varnothing \times \left(\frac{NTG}{100}\right) \times (1 - Sw)}{5.615 \times Bo}$$

---------- 3.7

Where, A = the surface area of a block, h = gross thickness (ft), NTG = net-to-gross ratio, ø = porosity, S_w = the water saturation and B_o = formation volume factor (res bbl/STB).

For example, a grid block with a porosity of 0.18802 (18.802%) and NTG of 86.2911%, the OOIP is calculated to be 0.0593 MMSTB.

Hence, the sum of the individual OOIP for each grid block gave the total OOIP for the model.

$$Total\,OOIP = \sum_{i=1}^{n} \frac{A \times h \times NTG \times \left(\frac{\varnothing}{100}\right) \times (1 - Sw)}{5.615 \times Bo}$$

---------- 3.8

Using this formula, the total oil in place for the entire model is estimated to be 523.2 MMSTB. The difference of this value from values to be estimated by reservoir model initialization or any other method may be attributed to the several parameters employed in computing the variograms which were then used for building the realizations.

3.7 Estimation of Horizontal and Vertical permeabilities.

Permeability distributions in the reservoir model were created using methods described in Section 3.4.1. Lognormal distributions were used to represent permeabilities. These permeability values are taken as the average permeability, k_{avg} such that:

$$k_{avg} = \sqrt[3]{k_X . k_Y . k_Z} \quad \text{---------- 3.9}$$

Then, using a range of kV/kH ratios, for instance 0.05, 0.20, 0.40, etc., it is derived that

$$k_{avg} = k_H . \sqrt[3]{x} \quad \text{---------- 3.10}$$

Where x = 0.05, 0.20, 0.40, etc.

The derivation of equation 3.10 is shown in Appendix C.

To obtain directional permeabilities, it is assumed that permeability in the y-direction is 80% of the permeability in the x-direction (Lach, 2010). Hence, horizontal permeability, k_H is calculated as:

$$k_H = \sqrt{k_X . k_Y} \quad \text{---------- 3.11}$$

Finally, permeability in the z – direction is calculated from equation 3.10 as :

$$k_z = k_V = \frac{k}{\frac{(¿¿avg)^3}{k_X . k_Y}} \quad \text{---------- 3.12}$$

3.8 Reservoir Simulation and Waterflood Performance Analysis

3.8.1 Reservoir Simulation Model Initialization

The T-1 reservoir model is an undersaturated reservoir with an initial average reservoir pressure of 11305 psia. The oil initially in place (OIIP) after initialization is put at 1.792 MMSTB. The other properties of the reservoir are stated in sections 3.4 and 3.5. There are 360 grid cells in the model, out of which 288 cells are active grid cells. There are also ten (10) layers in the reservoir, out of which eight (8) zones are reservoir sands – layers 1 and 2 were assumed to be shale bodies which contained no reserves. The effects of gravity segregation as well as fluid and rock compressibilities were included in the simulation runs of the model. The start time for the simulation was June 1, 1996.

3.8.2 Waterflooding of the T-1 Reservoir

Reservoir Development Plan

The production scheme used for this reservoir model involved two stages. Firstly, the development of the field began in June 1996, with just one producer with an oil flowrate of 1000STB/day for the five-spot pattern scenario, and two producers at oil rates of 500STB/day each for the scenarios of direct-line and staggered-line scenarios. Upon production, it was decided that waterflooding should be commenced after three (3) years of production and it was carried out for ten (10) years.

Waterflooding was carried out to increase and/or maintain reservoir pressure above bubble point (6306 psia), and to increase the oil producing rate of the field. Waterflooding started in June 1999 with four (4) injectors for each of the scenarios, all injecting at a rate of 700STB of water/day.

The injectors were positioned such the waterflood pattern approximated the regular five-spot, direct-line drive and staggered-line patterns corresponding to their respective scenarios.

These rates were used throughout the period of simulation. The economic limit for producers consists of 50STB/day for production rate and a maximum water-cut of 0.95. This production strategy was used for analysis of the effects of kV/kH ratio and zones of injection /production (ZoIP) on waterflooding. As earlier stated, comparisons of waterflood performance were based on field average reservoir pressure (FPR), cumulative oil production (FOPT), and field water-cut (FWCT) for a period of thirteen (13) years (3 years of primary depletion and 10 years of waterflooding).

Methodology for Analyzing the Effects of kV/kH Ratio (kVkH) on Waterflood Performance

Four kV/kH ratios were selected and their effect on the waterflood performance was analyzed. They were:

- k_V/k_H ratio of 0.001 **(kVkH_0.001),**
- k_V/k_H ratio of 0.01**(kVkH_0.01),**
- k_V/k_H ratio of 0.10 **(kVkH_0.1),** and
- k_V/k_H ratio of 0.60**(kVkH_0.60).**

The base case of the kV/kH ratios was 0.6. These were done for the regular five spot, direct-line drive and staggered-line drive patterns. Water was injected in zones 6 – 8, and the producers were completed in zones 4 – 6.

Waterflood Optimization

In defining a reservoir optimization problem, an objective function, optimization variables and their constraints should be specified (Asadollahi, 2012). Objective functions for waterflood optimization include net pressure value (NPV), cumulative production or delay in water breakthrough/ reduction in water-cut while controlling variables such as injection rate, oil production rate and/ or bottom-hole pressure of injectors and producers.

For this research, waterflood optimization aimed at increasing cumulative oil production while taking into consideration the zones of water injection and oil production and the pattern of waterflood i.e.:

$$Cumulative\ oil\ production = f\left(Zones\ of\ water\ injection, zones\ of\ oil\ production, Pattern\ of\ waterflood\right)$$

Methodology for Analyzing the Effects of Zones of Injection and Production (ZoIP) on Waterflood Performance

The simulation was carried out for 13 years – 3 years of primary depletion and 10 years of waterflooding. In so doing, the effect of zones of injection as well as production on the reservoir performance was analyzed. The cases chosen are explained below:

- **Case 1 (NO_WF):** For this case, primary production was done using reservoir depletion mechanism and waterflooding was not considered. This was done to ascertain the best time to begin waterflooding. The wells were completed in zones 4 – 6.
- **Case 2 (ALL_ZONES):** This case involved waterflooding after three years of primary production. Production was carried out from six zones, – layers 3 to 8 and water was injected into all zones of the reservoir including the aquifer zones, – layers 3-10.
- **Case 3 (AQUIFER):** This case also involved waterflooding with optimization in which production was carried out from three zones, – layers 6 to 8, and water was injected into the aquifer zones, – layers 9 and 10.
- **Case 4 (ZONES_6-8):** Here, production was carried out from three zones, – layers 4 to 6, and water was injected in three zones, – layers 6 to 8.

These ZoIP scenarios were carried out for the regular five spot, direct-line drive, and staggered-line drive patterns. Figures 3.8 - 3.10 show schematics of the scenarios considered.

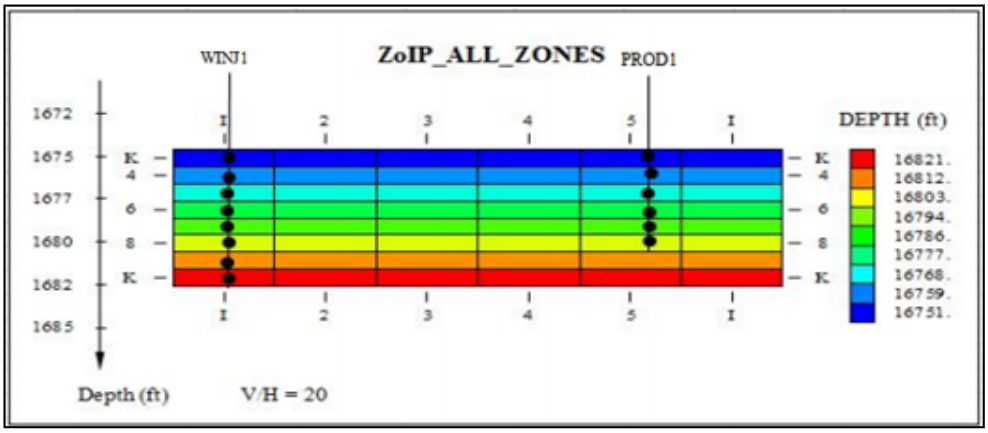

Figure 3.13: Cross Section of the T-1 reservoir showing completion of an injector in all zones of the reservoir and a producer in six zones.

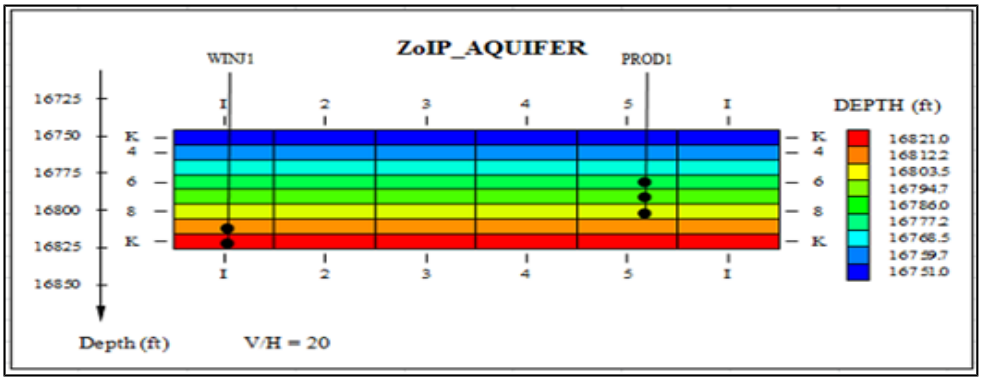

Figure 3.14: Cross Section of the T-1 reservoir showing completion of an injector in the aquifer zone and a producer in zones 6-8.

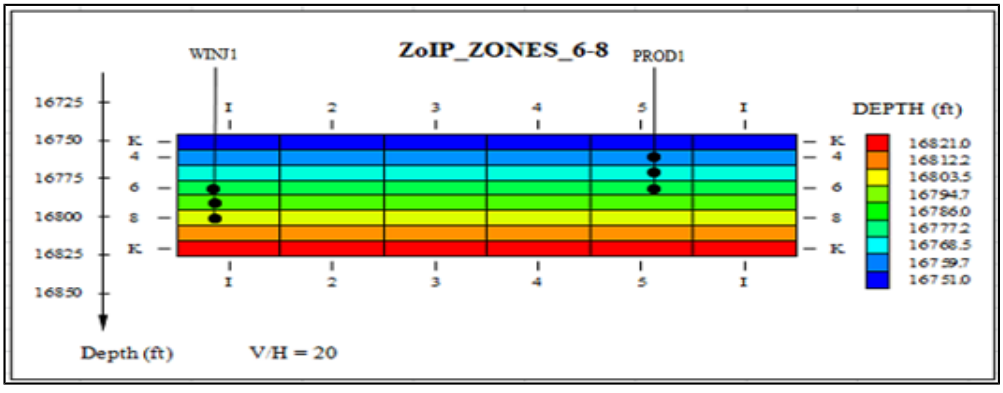

Figure 3.15: Cross Section of the T-1 reservoir showing completion an injector in zones 6-8 and a producer in zones 4-6.

Another important reason for carrying out a study on the effect of the zones of production and injection was to ascertain the best zones for completing the injectors and production, to get optimal oil production and water injection. This was used for further analyses in this research.

Methodology for Analyzing the Effects of Waterflood Pattern (PoWF) on Waterflood Performance

To select the optimal waterflood pattern for producing the T-1 reservoir, it was necessary to analyze the performance of several waterflood patterns. All producers were completed in three zones – layers 4 to 6, and water was injected in three zones only – layers 6 to 8. This conclusion was reached based on results obtained from the ZoIP Cases. The scenarios analyzed were the five-spot pattern (5_SPOT), the direct-line drive pattern (LD) and the staggered line drive pattern (SLD).

For the five-spot pattern, the distance between all the injectors was constant. The four injectors formed a square with the production well in the center. In the direct-line drive pattern, the lines of injection and production were directly opposite each other. For the staggered line-drive pattern, the wells are in line similar to the direct-line drive pattern with the same injection and production rate. However, the injectors and producers are no longer directly opposed to each other but laterally displaced.

Also, the injectors and producers for all the patterns considered were constrained so that total injection rate for all the injectors was 2800stb/day of water, and the total production rate from the producers was 100stb/day. This was done so as to provide a basis for comparison.

The comparison of the results obtained from all the kV/kH, ZoIP and PoWF cases is done using field average reservoir pressure (FPR), field cumulative oil production (FOPT) and field water-cut (FWCT). The results of these analyses are presented and discussed in the next chapter.

CHAPTER 4

RESULTS AND DISCUSSION

4.1 Introduction

Simulations involving the cases illustrated in section 3.7.2 were carried out. The results obtained from the waterflooding of the T-1 reservoir are presented in this chapter. The analysis of these results is discussed and observations derived from the results are also included in this chapter.

The results showing the effect of kV/kH ratios on waterflood performance are compared and discussed first. The results from the waterflood optimization are then compared and discussed.

4.2 Analysis of Waterflood Performance

4.2.1 Effects of kV/kH Ratios on Waterflood Performance

Presented in the following sections are results showing the effect of variation in the ratio of vertical-to-horizontal permeability on waterflood performance. The presented pattern scenario is the regular five-spot pattern. The results for the direct-line and staggered-line drive are also presented and analyzed.

Effects of kV/kH Ratios on Cumulative Oil Production (FOPT)

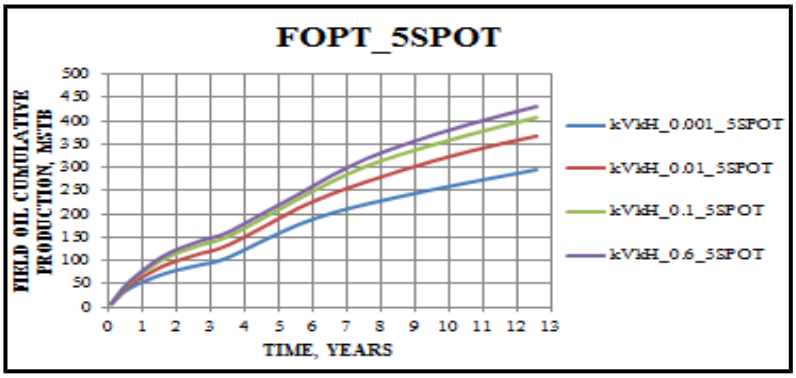

Figure 4.1: Plot of cumulative production vs. time for different k_V/k_H ratios for the 5-spot pattern.

Figure 4.1 is a plot of cumulative oil production vs. time for the five-spot waterflood considering four kV/kH ratios – 0.001, 0.01, 0.1 and 0.6. Note that waterflood for each kV/kH ratio was simulated for ten (10) years. The results show that cumulative oil production improves with increasing kV/kH ratio (with approximately 300MSTB, 360MSTB, 405MSTB and 425MSTB for the kV/kH ratios scenarios of 0.001, 0.01, 0.1 and 0.6 respectively). This is because the sweep efficiency of the waterflood improves with better k_V/k_H ratio. This is due to improved crossflow/ fluid transmissibility between layers from non-depleted zones to already depleted zones within the reservoir. Better sweep efficiency could also lead to lower water-cut which was observed for these cases at the end of the simulation.

Figure 4.2 shows a plot of cumulative oil production vs. time for the direct-line drive waterflood considering four kV/kH ratios – 0.001, 0.01, 0.1 and 0.6 simulated for thirteen years – 3 years of primary depletion and 10 years of waterflood.

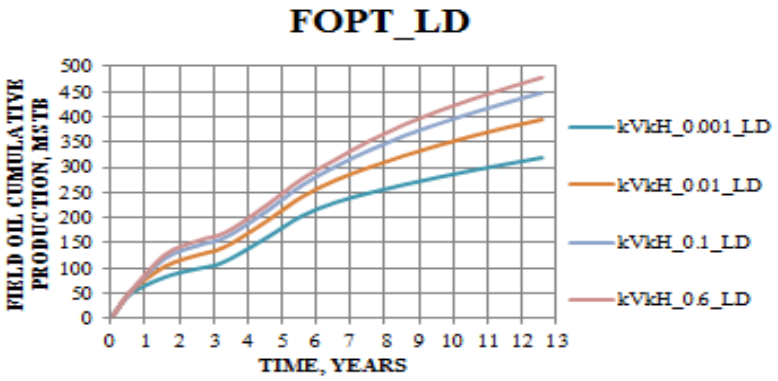

Figure 4.2: Plot of cumulative production vs. time for different k_V/k_H ratios for the direct-line drive waterflood.

Similar to the results obtained from the five-spot pattern, it is observed that cumulative oil production improves with increasing kV/kH ratio.

Even though the total production rate from the wells was fixed at 1000stb/day (500stb/day from each well) and total injection rate at 2800 stb/day (700stb/day for each injector), it is observed that cumulative production at the end of simulation for all the kV/kH cases analyzed is higher compared to that obtained from the 5-spot scenario (with one producer producing at 1000stb/day and four injectors injecting at 700stb/day). This is because the two producers (for the direct line-drive) had an advantage over one producer (for the 5-spot) in that, more zones of the reservoir were available for drainage by the producers.

Figure 4.3 is a plot of cumulative oil production vs. time for the staggered-line drive waterflood considering four kV/kH ratios – 0.001, 0.01, 0.1 and 0.6 simulated for thirteen years – 3 years of primary depletion and 10 years of waterflood. Here, the wells are in line as in, the direct-line drive pattern with the same injection and production rate.

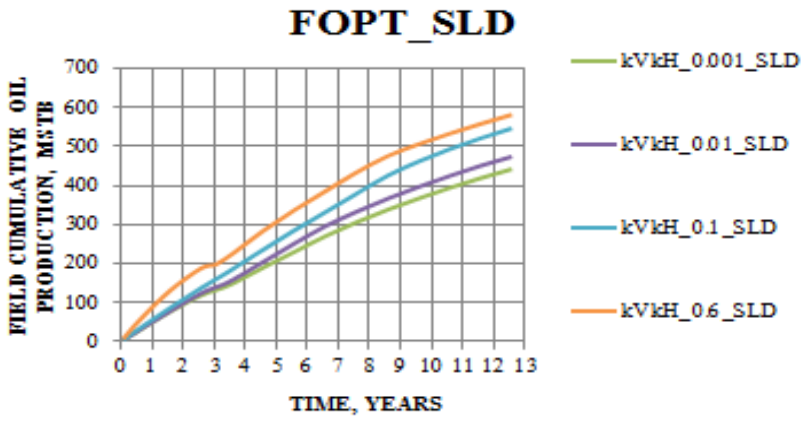

Figure 4.3: Plot of cumulative production vs. time for different k_V/k_H ratios for the staggered-line drive waterflood.

The results are similar to those obtained for the previous patterns as it is observed that cumulative oil production improves with increasing kV/kH ratio. However, the staggered-line drive pattern is observed to give the highest cumulative recovery for all kV/kH ratios considered, than the previous waterflood scenarios (with approximately 430MSTB, 480MSTB, 520MSTB and 580MSTB for the kV/kH ratios scenarios of 0.001, 0.01, 0.1 and 0.6 respectively). This is

because the lateral displacement of the injectors to the producer ensures that larger areas of the reservoir are contacted by the injected water and hence better sweep of oil towards the producers.

Effects of kV/kH Ratios on the Field Oil Producing Rate (FOPR)

Figures 4.4 through to 4.6 show plots of oil producing rate of the field vs. time for the five-spot, direct-line drive and the staggered line-drive waterfloods considering four kV/kH ratios – 0.001, 0.01, 0.1 and 0.6. This simulation was carried out for thirteen (13) years – three (3) years of primary production and ten (10) years of waterflood. As earlier stated, the total production rate from the wells was fixed at 1000stb/day (1000stb/day for the five-spot waterflood and 500stb/day for the two wells employed in the direct and staggered line-drive waterflood) and the total injection rate at 2800 stb/day (700stb/day for each injector) for all waterflood scenarios.

Generally, it is seen that cases with lower kV/kH ratios have lower oil production rates when compared to cases with higher kV/kH ratios. This is because for reservoirs with low vertical-to-horizontal permeability ratios, there is poor reservoir fluid transmissibility in the vertical direction from one zone to another. This results in poor mobility/ sweep efficiency of the injected water and hence lowers oil production rates.

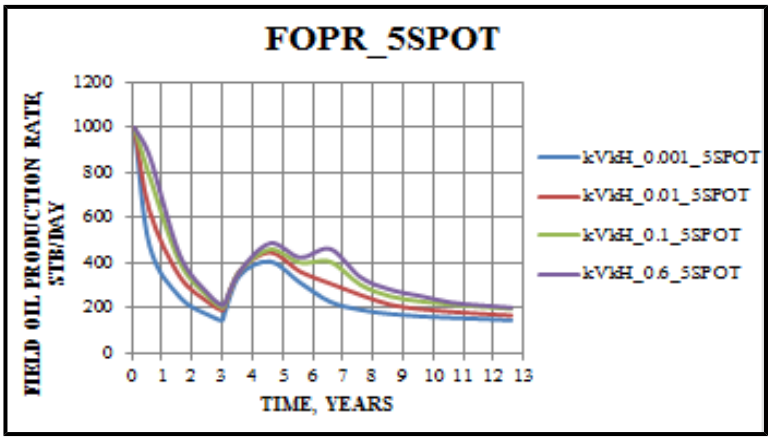

Figure 4.4: Plot of Plot of field oil production rate vs. time for different k_V/k_H ratios for the 5-spot pattern.

However, cases with higher kV/kH ratios show higher oil producing rates compared to cases with lower kV/kH ratios. This due to good lateral transmissibility between layers as a result of good communication between zones in the reservoir.

Figure 4.5 shows a plot of oil production rate vs. time for the direct-line drive waterflood considering four kV/kH ratios – 0.001, 0.01, 0.1 and 0.6. The results obtained are similar to the results obtained from the five-spot pattern as it is observed that oil production rates improve as the kV/kH ratio increases.

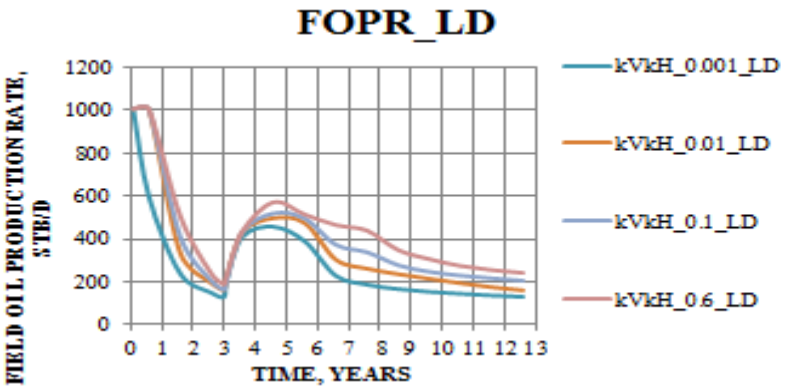

Figure 4.5: Plot of field oil production rate vs. time of different k_V/k_H scenarios for the direct-line drive pattern.

However, the production rates for the four kV/kH ratios – 0.001, 0.01, 0.1 and 0.6 analyzed is observed to be corresponding higher than those of the five-spot scenario throughout the period of simulation. This is because, even though the total production rate from the wells were constrained (fixed at 1000stb/day (500stb/day from each well), and total injection rate at 2800 stb/day (700stb/day for each injector)), two producers (for the direct line-drive) still had an advantage over one producer (for the 5-spot) since more zones of the reservoir were available for drainage by the producers and oil could flow from zones around the depleted zones to replenish them.

Figure 4.6 shows a plot of oil production rate vs. time for the staggered-line drive waterflood. Similarly, the oil production rate is found to increase with the kV/kH ratio. However, upon waterflooding, the staggered-line drive pattern is observed to give the highest rate for all kV/kH ratios considered when compared to the other waterflood scenarios. This is because the lateral positioning of the injectors to the producer ensures that larger areas of the reservoir are contacted by the injected water, and hence better sweep of oil towards the producers.

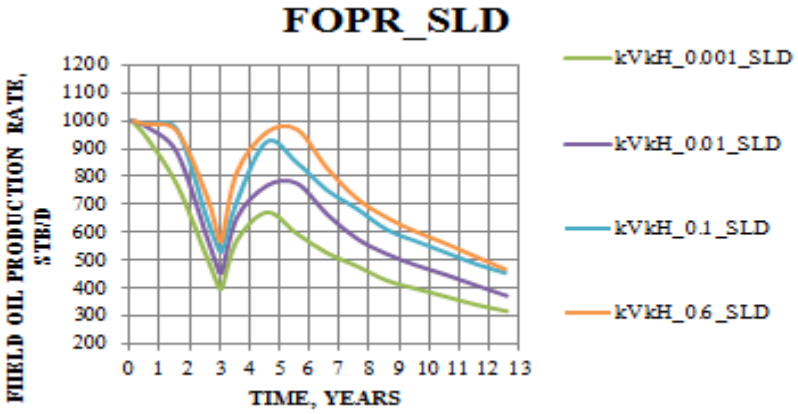

Figure 4.6: Plot of field oil production rate vs. time of different k_V/k_H scenarios for the staggered-line drive pattern.

Effects of kV/kH Ratios on Reservoir Pressure (FPR)

Figure 4.7 is a plot of average reservoir pressure of the T-1 reservoir vs. time for the five-spot waterflood considering four kV/kH ratios – 0.001, 0.01, 0.1 and 0.6. Waterflood for each kV/kH ratio was simulated for ten (10) years. From the figure, it is observed that higher kV/kH ratios showed lower pressure decline. Case kVkH_0.60 has the lowest pressure decline, while Case kVkH_0.001 has the highest pressure decline throughout the period of simulation. This can be attributed to the fact that there is little communication between the zones for reservoirs with low kV/kH ratios and hence lower pressure maintenance. Recall that water injected moves preferentially in the vertical upwards direction due to gravity. A high kV/kH ratio implies good vertical communication between reservoir zones and hence easier movement of injected water

vertically. This results in better pressure maintenance. Also, the injected water would flow into non-injected zones, thus improving pressure maintenance.

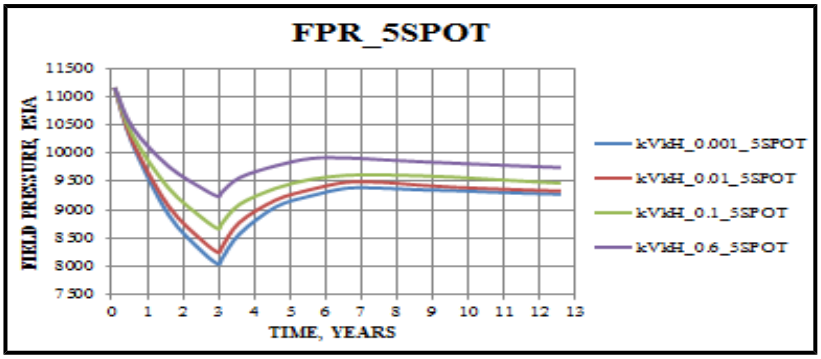

Figure 4.7: Plot of average field pressure vs. time of different k_V/k_H scenarios of the five-spot waterflood.

Similar trends are observed for the plots for the direct line-drive and the staggered line-drive scenarios shown in Figures 4.8 – 4.9.

Figure 4.8 is a plot of field pressure vs. time for the direct-line drive waterflood for the four kV/kH ratios considered– 0.001, 0.01, 0.1 and 0.6. From the figure, it is observed that the trend in reservoir pressure is lower than that of the five-spot waterflood. This is due to the fact that, even though both waterfloods have an equal number of injectors (injecting at the same total field injection rate of 2800stb/day), the number of producers are different (one for the five-spot and two for the direct-line drive).

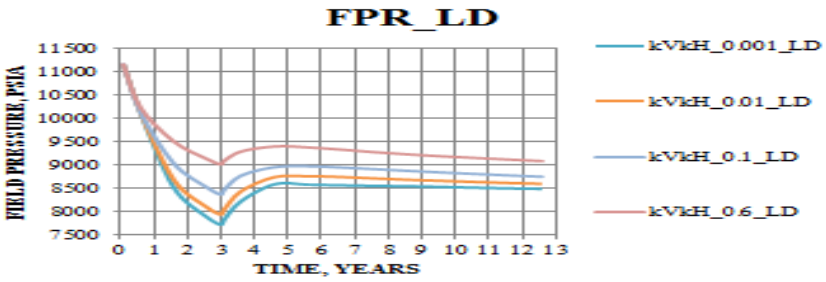

Figure 4.8: Plot of field oil production rate vs. time of different k_V/k_H scenarios for the direct-line drive pattern.

Figure 4.9shows a plot of field pressure vs. time of the four kV/kH ratios considered– 0.001, 0.01, 0.1 and 0.6 for the staggered-line drive waterflood. Like the direct-line waterflood, there are four injectors (injecting at a total field injection rate of 2800stb/day) and two producers (with total oil rate of 1000stb/day).

It is observed that the trend in reservoir pressure after waterflooding is correspondingly higher than those of the previous waterflood patterns considered. This is because of the lateral orientation of the injectors to the producers. This allows for effective displacement of injected water and hence better pressure maintenance.

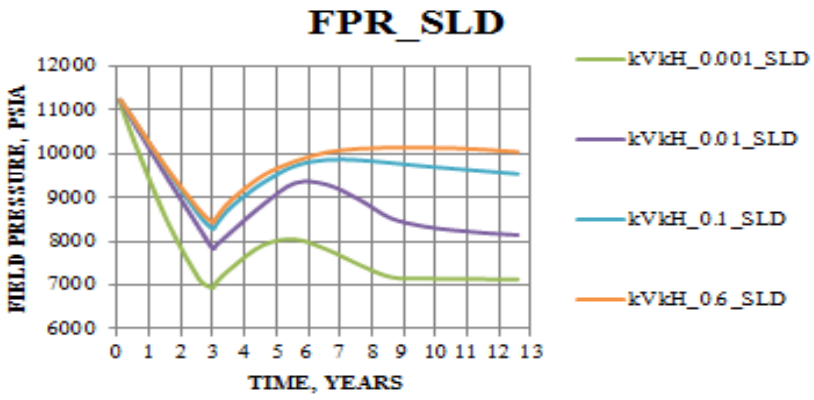

Figure 4.9: Plot of field pressure vs. time of different k_V/k_H scenarios for the staggered-line drive pattern.

Effects of kV/kH Ratios on Field Water-Cut (FWCT)

Figure 4.10 – 4.12 show a plot of field water-cut vs. time of all the kV/kH cases studied for the five-spot, direct-line drive, and staggered-line drive waterfloods respectively. It is seen that for all the waterflood scenarios analyzed, all kV/kH cases showed no significant water-breakthrough prior to waterflooding until around five (5) years of production. The trend of field water-cut for all the scenarios of waterflood considered, is observed to be similar with the highest water-cut of less than 80% at the end of the simulation. This is because the number of injectors and the injection rate for each scenario is the same.

Also observed is that that for all scenarios, increasing kV/kH ratios leads to higher water-cut. This is because the sweep efficiency in all zones improves with increasing kV/kH ratios since there is increased communication between the zones. This can substantially increase water production at the producers and subsequently, field water-cut. For cases of very low kV/kH ratios (kVkH_0.001 and kVkH_0.01), there is poor communication between zones and hence, lower water production.

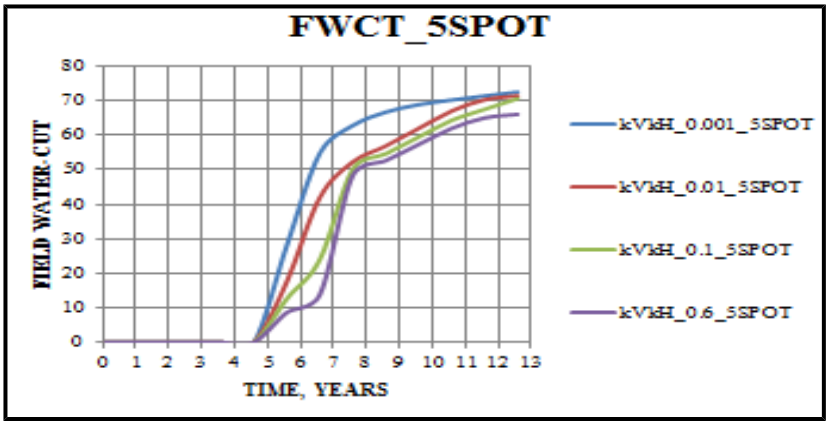

Figure 4.10: Plot of field water-cut vs. time for different k_V/k_H scenarios for the five-spot pattern.

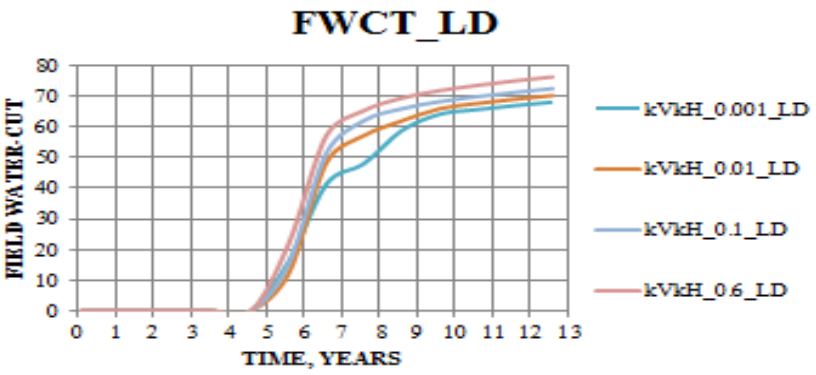

Figure 4.11: Plot of field water-cut vs. time of different k_V/k_H scenarios for the direct-line drive pattern.

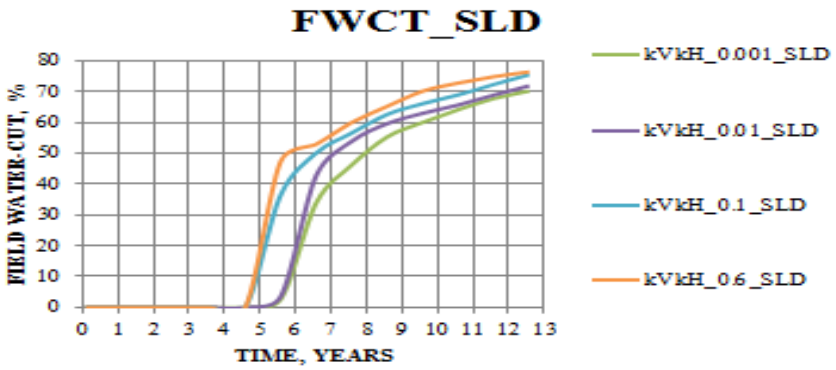

Figure 4.12: Plot of field water-cut vs. time of different k_V/k_H scenarios for the staggered-line drive pattern.

4.3 Waterflood Optimization

These sections present the results of the optimization procedure discussed in Section 3.7.2.

4.3.1 Effects of Zones of Production and Injection on Waterflood Performance

In this section, the effect of zones of injection and production on the reservoir's primary depletion and waterflood performance was analyzed. This was done in order to ascertain the best zones for completing of the injectors and production so as to get optimal oil production and water injection. Results from this study were used in analyses of patterns of waterflood to be adopted. From results obtained, it was seen that injecting and producing from some zones was optimal compared to other zones. Hence, the zones of completion of injectors and producers play a vital role in waterflood performance. The pattern discussed is the regular five-spot pattern. The results for the direct-line and staggered-line drive are presented here for comparison to the flood performance. The following scenarios were considered:

1. Case ALL_ZONES in which water was injected into all zones of the reservoir and production was carried out from all producible zones; (zones 3-8).
2. Case AQUIFER in which water was injected into the aquifer zones and the producers were completed in zones 6 – 8.

3. Case ZONES 6 – 8 in which water was injected into zones 6 – 8 and oil was produced from zones 4 – 6.
4. Case NO_WF in which the producers were completed in zones 4 – 6.

Effects of ZoIP on Field Cumulative Oil Production (FOPT)

Figures 4.13 – 4.15 are plots of cumulative oil production vs. time of all the ZoIP cases analyzed (Cases ALL-ZONES, AQUIFER, ZONES 6-8 and NO_WF) for the five-spot, direct-line drive and the staggered line-drive waterfloods respectively considering three cases of ZoIP. Note that simulation was carried out for thirteen (13) years – three (3) years of primary production and ten (10) years of waterflood. It is observed that cumulative oil production for all cases increases with time within the cases of injection into all zones and zones 6-8 showing the highest increase.

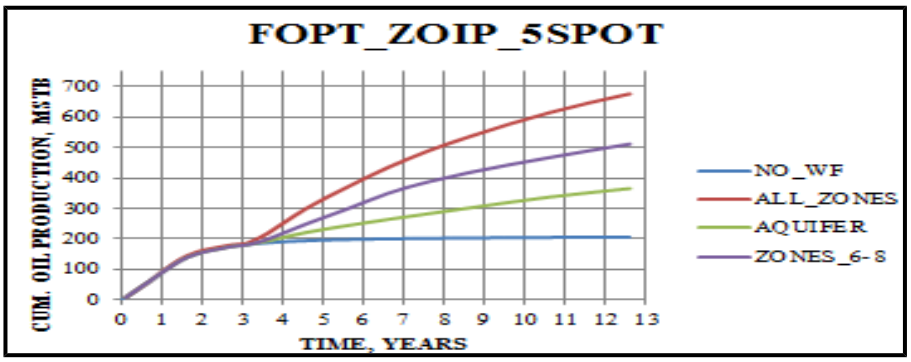

Figure 4.13: Plot of field cumulative production vs. time for the ZoIP scenarios for the five-spot waterflood.

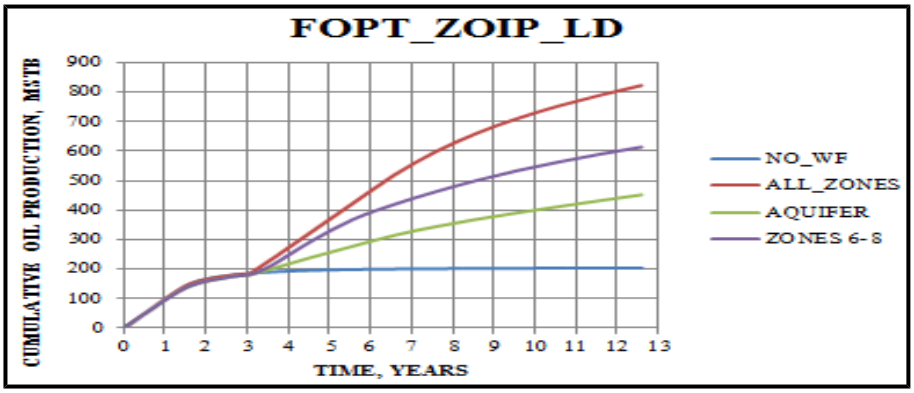

Figure 4.14: Plot of field cumulative production vs. time for different ZoIP scenarios for the direct-line drive waterflood.

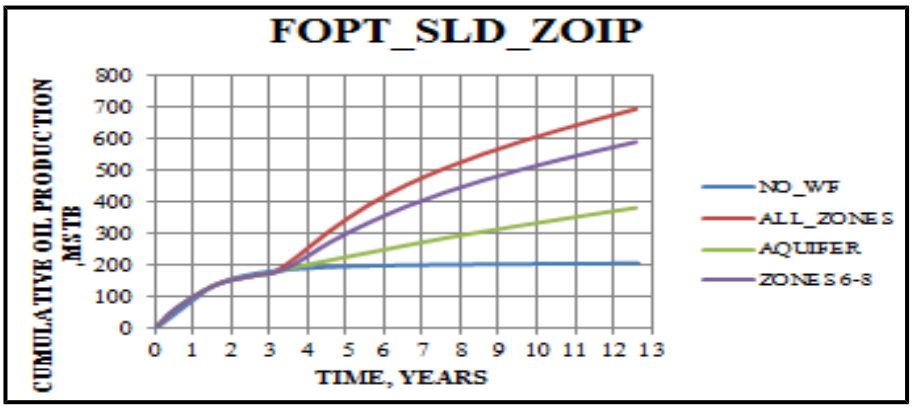

Figure 4.15: Plot of field cumulative production vs. time for different ZoIP scenarios for the staggered-line drive waterflood.

As expected, the case which involved no water injection had the lowest cumulative recovery. Case AQUIFER gives the lowest cumulative production for all cases of waterflooding considered.

Also, the direct-line and staggered-line drive waterflood are observed to have higher cumulative recovery than the five-spot waterflood for corresponding ZoIP cases. This is because the two producers (for the direct line-drive and staggered line-drive waterfloods) have an advantage over one producer (for the 5-spot), meaning that more zones of the reservoir were available for

drainage by the producers. Also, when water injectivity is low or in heterogeneous reservoir systems like the T-1 reservoir, line-drive is favored to improved recovery.

Finally, the direct-line drive waterflood is also observed to have the highest cumulative than that of other waterflood in corresponding ZoIP cases.

Effects of ZoIP on the Field Oil Production Rate (FOPR)

Figures 4.16 through 4.18 show plots of the oil producing rate of the field vs. time for the five-spot, direct-line drive and the staggered line-drive waterfloods respectively considering three cases of ZoIP. The total production rate for the producers were fixed at 1000stb/day (1000stb/day for the five-spot waterflood, and 500stb/day for the two wells employed in the direct and staggered line-drive waterflood), and the total injection rate at 2800 stb/day (700stb/day for each injector) for all waterflood scenarios.

The plots show that the reservoir production is more effective when all zones of the reservoir can produce oil and inject water, with Case ALL_ZONES having the highest cumulative oil production for all periods after waterflooding. This is because production is largely a function of voidage. The more the zones injecting water, the higher the voidage replacement of reservoir fluids and thus, a decline in production rate is curtailed. However, this is not good practice as it can also lead to very high water production.

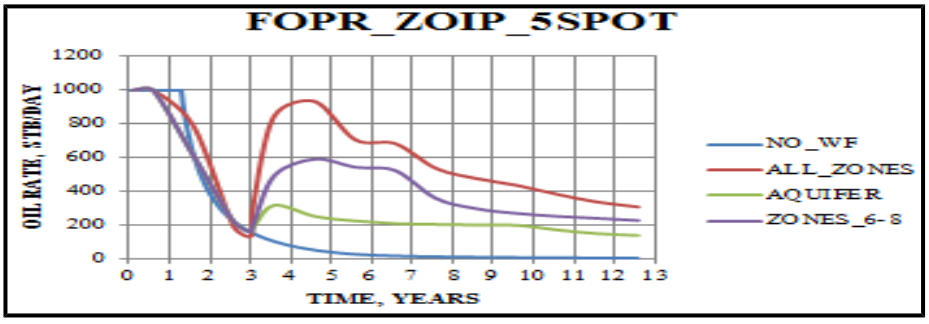

Figure 4.16: Plot of field oil production rate vs. time for different ZoIP scenarios for the five-spot waterflood.

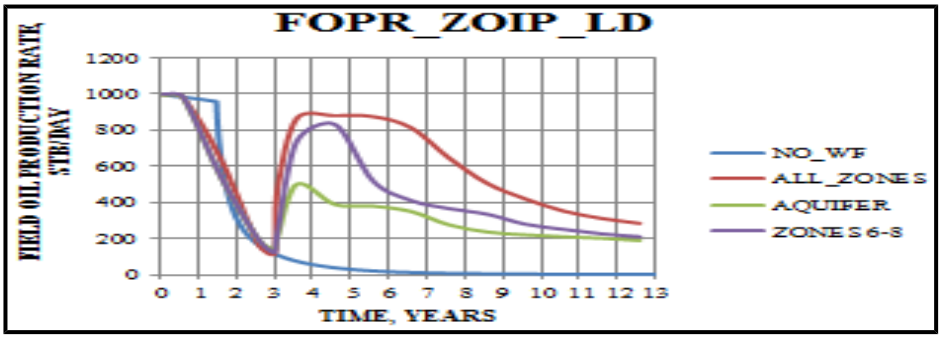

Figure 4.17: Plot of field oil production rate vs. time for different ZoIP scenarios for the direct-line drive waterflood.

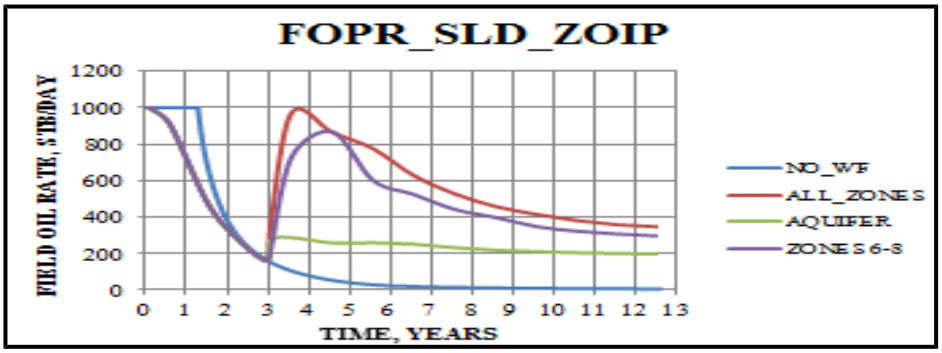

Figure 4.18: Plot of field oil production rate vs. time for different ZoIP scenarios for the staggered-line drive waterflood.

Also, injection into zones 6, 7 and 8 (ZoIP_6 - 8) is seen to give higher production rates than the case of water injection into the aquifer (AQUIFER). This is because injection into oil-bearing zones in the reservoir tends to displace more oil towards the producers than injection into the aquifer.

Effects of ZoIP on Field Water-Cut (FWCT)

Figures 4.19 – 4.21 are plots of field water-cut vs. time of all the ZoIP cases analyzed (Cases ALL-ZONES, AQUIFER, ZONES 6-8 and NO_WF) for the five-spot, direct-line drive and the staggered line-drive waterfloods respectively considering three cases of ZoIP.

It is observed that for all waterflood scenarios analyzed, none of the ZoIP cases considered had a significant amount of water production prior to waterflooding.

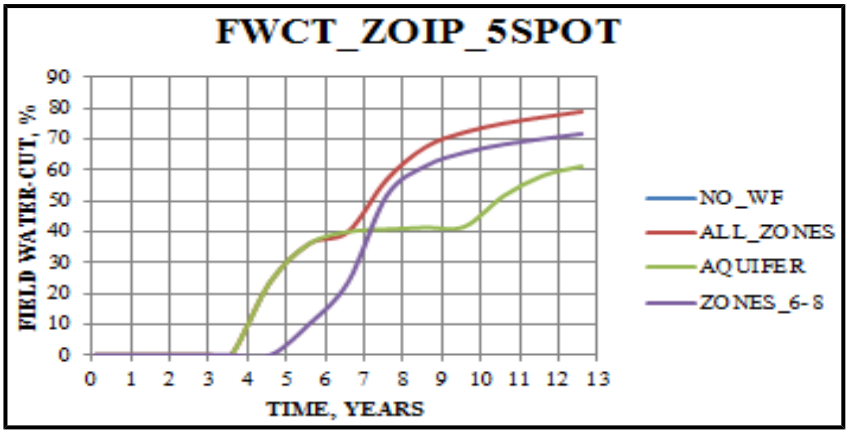

Figure 4.19: Plot of field water-cut vs. time for different ZoIP scenarios for the five-spot waterflood.

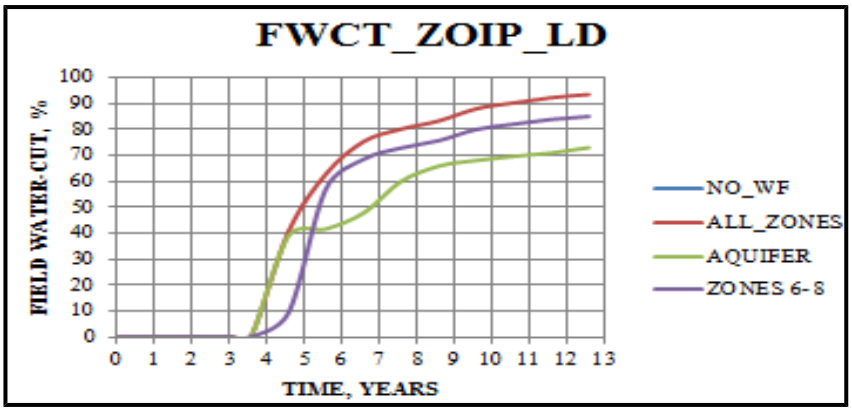

Figure 4.20: Plot of field water-cut vs. time for different ZoIP scenarios for the direct-line drive waterflood.

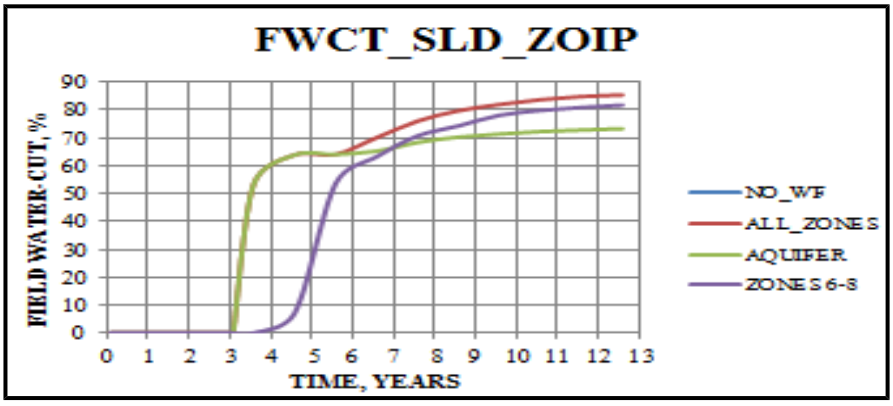

Figure 4.21: Plot of field water-cut vs. time for different ZoIP scenarios for the staggered-line drive waterflood.

Also observed is that injecting water into fewer zones leads to a reduction in water production. Injection of water into all the zones in the reservoir will lead to an increase in water production. It is seen that injection of water into zones other than the aquifer would result in high water-cut. This is because injection into such zones can cause a higher production of water with displaced oil.

Finally, water injection into the aquifer (case AQUIFER) is seen to have the least water production for all cases considered.

Effects of ZoIP on Field Pressure (FPR)

Figure 4.22 – 4.24 show plots of field pressure vs. time for the five-spot, direct-line drive and the staggered line-drive waterfloods respectively considering three cases of ZoIP. It is observed that for the staggered line drive, the trend in reservoir pressure after waterflooding is correspondingly higher than those of the previous waterflood patterns considered. This is because of the lateral orientation of the injectors to the producers. This allows for effective displacement of injected water and hence better pressure maintenance.

Also observed is that pressure maintenance/ increment is more effective when more zones of the reservoir can inject water. This is because pressure decline is largely a function of voidage. If more zones in the reservoir are injecting water, there is voidage replacement and thus pressure decline is arrested.

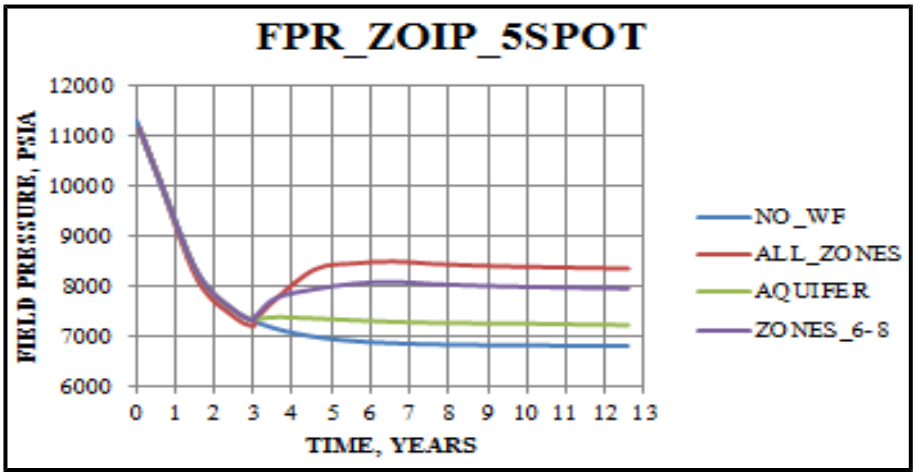

Figure 4.22: Plot of field pressure vs. time for different ZoIP scenarios for the five-spot waterflood.

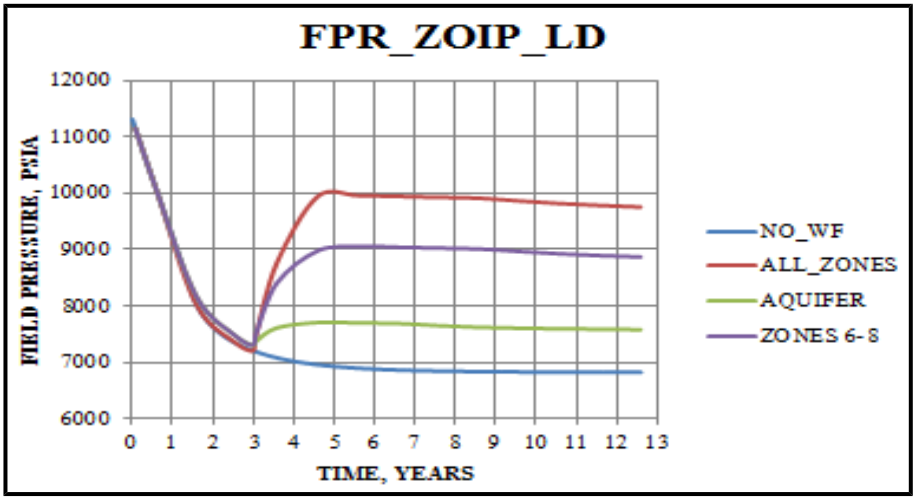

Figure 4.23: Plot of field pressure vs. time for different ZoIP scenarios for the direct-line drive waterflood.

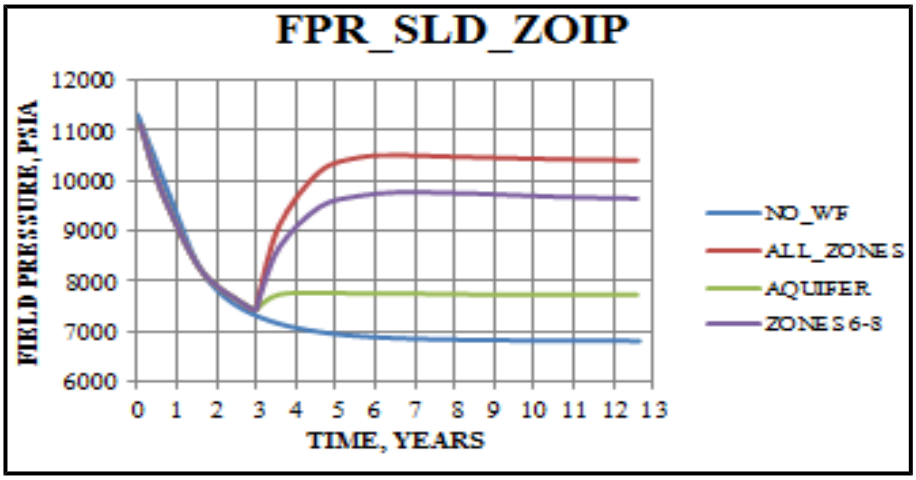

Figure 4.24: Plot of field pressure vs. time for different ZoIP scenarios for the staggered-line drive waterflood.

Finally, injection of water into zones 6, 7 and 8 (case ZONES 6-8) is seen to give higher pressure increment than the case which involved injection into the aquifer. It is also observed that injection into the aquifer (case AQUIFER) has no significant pressure maintenance effect as reservoir pressure is still observed to decline.

4.3.2 Effects of Waterflood Patterns on the Performance of the Waterflood

In this section, the impact of the selected waterflood patterns on waterflood performance is evaluated. This is done by analyzing trends in the field oil production rate, field water-cut, cumulative production and field reservoir pressure. The optimal pattern would be that pattern which would give the highest cumulative production with appreciable low water-cut.

Effects of Selected Waterflood Patterns on the Field Cumulative Production (FOPT)

Figure 4.25 is a plot showing the effect of the selected flood pattern on the cumulative oil production from the field. The simulation was carried out for thirteen (13) years – three (3) years of primary production and ten (10) years of waterflood.

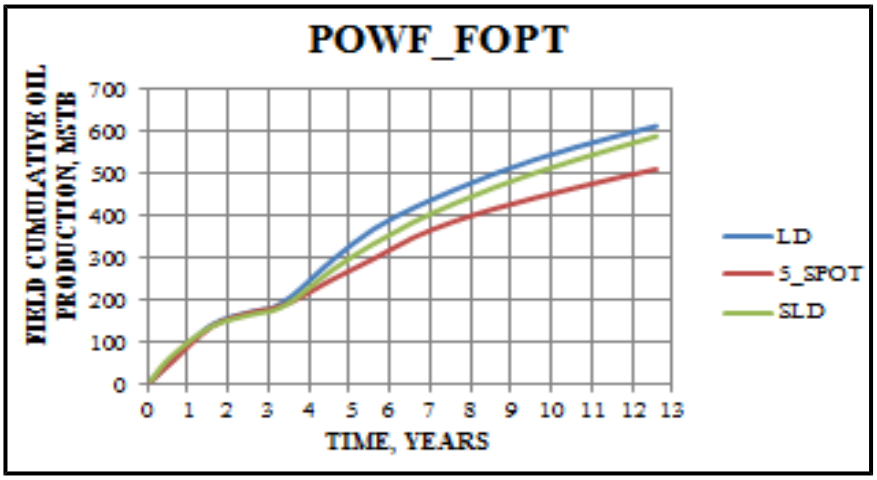

Figure 4.25: Plot of field cumulative production vs. time for different PoWF scenarios.

It is observed that Case LD (direct-line drive pattern) gives the highest cumulative production for all scenarios analyzed. This is due to the efficient displacement of oil towards the producers by the injectors. In contrast, the Case 5spot (regular five-spot pattern) has a low cumulative production largely due to the absence of sufficient producers to produce displaced oil.

Waterflood Patterns to Choose for Optimum Field Oil Production Rate (FOPR)

Figures 4.26 is a plot of oil production rate of the field vs. time for the three patterns of waterflood considered – the five-spot, direct-line drive, and the staggered line-drive waterfloods respectively. The total production rate for the producers were fixed at 1000stb/day (1000stb/day for the five-spot waterflood and 500stb/day for the two wells employed in the direct and staggered line-drive waterflood) and the total injection rate at 2800 stb/day (700stb/day for each injector) for all waterflood scenarios. The producers are completed in zones 4 – 6 while the injectors are completed in zones 6 – 8.

It is clearly observed from Figure 4.27 that for all flood/injection patterns evaluated, there were corresponding effects in the field oil production rate.

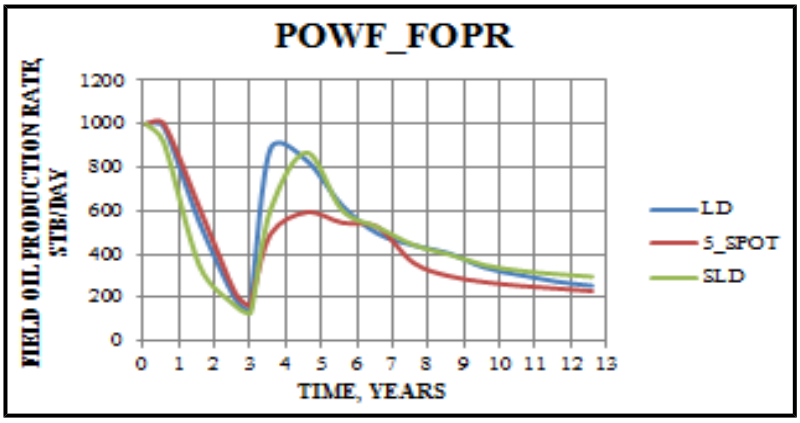

Figure 4.26: Plot of the production rate of the field with time for different PoWF scenarios.

Also, Cases LD (direct- line drive scenario) and SLD (staggered-line drive) are observed to have higher oil production rates for periods after waterflooding. This is because the field was adequately furnished with producers which helped drain the reservoir and injectors which ensured that oil was sufficiently displaced towards these producers, hence maintaining the high oil rate observed. Also, the placement of the injectors in line with the producers allows for efficient displacement of oil by the advancing water front.

Finally, it is observed that the case 5_Spot (a regular five-spot waterflood scenario) has the lowest oil rate of all the scenarios. This is due to the lack of sufficient producers which would adequately drain the reservoir. This is because the two producers (for the direct line-drive and staggered line-drive patterns) have an advantage over one producer (for the 5-spot) meaning more zones of the reservoir were available for drainage by the producers.

Effects of Selected Waterflood Pattern on Field Water-Cut (FWCT)

Figures 4.27 is a plot of water-cut of the field vs. time for the three patterns of waterflood considered – the five-spot, direct-line drive, and the staggered line-drive waterfloods respectively. Note that simulation was carried out for thirteen (13) years – three (3) years of primary production and ten (10) years of waterflood.

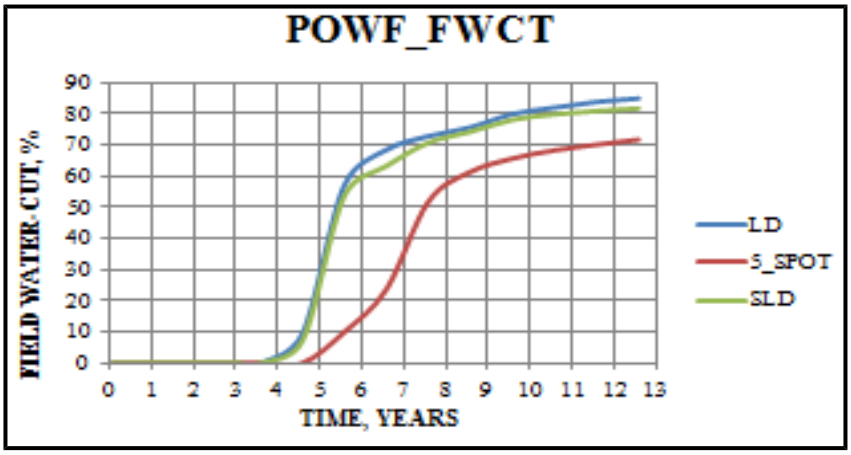

Figure 4.27: Plot of field water-cut vs. time for different PoWF scenarios.

It is observed that Case LD (the direct –line drive pattern) and Case SLD (the staggered-line drive pattern) have similar water-cut trends which are higher than that of the five-spot waterflood pattern. This is due to the placement of the injectors in line with the producers in distance closer than those obtainable for the five-spot waterflood pattern and allows for the faster movement of the advancing water front towards the producers and hence higher water production and earlier water breakthrough.

Also, the five-spot waterflood scenario has the least water-cut throughout the period of simulation. This is because of the distance between the injectors and the producer in this case as compared with the other cases. This causes late water-breakthrough and lower water production.

Effects of Selected Waterflood Pattern on Field Pressure (FPR)

Figure 4.28 is a plot of field pressure vs. time for the scenarios of waterflood patterns considered - the five-spot, direct-line drive and the staggered line-drive waterfloods. From the figure, it is observed that the plots for the line drive patterns have higher pressure profiles than the five-spot patterns after waterflooding. This is largely due to the shorter distances between the injectors and the producers for these patterns as compared to the five-spot patterns.

Also, Case SLD (the staggered-line drive waterflood) shows the highest pressure increment after waterflooding for all patterns analyzed. This is because the lateral orientation of the injectors to the producers allows for effective displacement of injected water and hence better pressure maintenance.

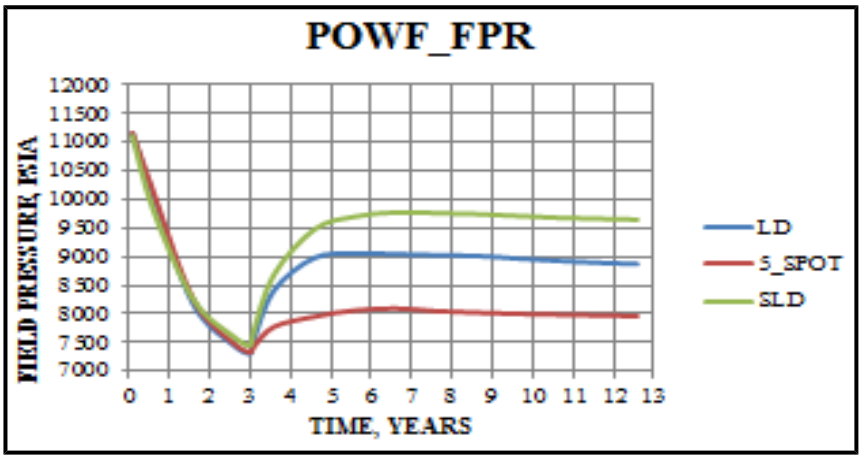

Figure 4.28: Plot of average field pressure vs. time for different PoWF scenarios.

CHAPTER 5

CONCLUSIONS AND RECOMMENDATIONS

5.1 Introduction

This chapter presents the various conclusions drawn based on results obtained from this study. Recommendations are also included to present areas for further research. The methodology presented and discussed by this research can be applied to develop the entire field.

5.2 Conclusions

1. Reservoir lateral and vertical heterogeneity affects injection and production from an oil-bearing system. The more heterogeneous a reservoir is, the more difficult it is to analyze injection and production from these systems.
2. It is observed that kV/kH ratio affects waterflood performance. A high kV/kH ratio across a reservoir implies a less likelihood of vertical cross-flow between layers. This results in a better sweep in high permeable, less heterogeneous zones. This could lead to better pressure maintenance and improved recovery.
3. The optimal waterflood pattern is that which results in higher recovery with corresponding low water-cut and late water breakthrough time. The direct-line waterflood pattern is chosen as the optimal pattern for this study.

5.3 Recommendations

1. A more robust optimization procedure would involve the consideration of NPV analysis to ascertain the viability of the methods proposed by this research. This can be undertaken as further research.
2. It is also recommended that further study should consider the orientation of the horizontal wells based on directional permeability to boost production.
3. In this research, the impact of injection and production efficiencies at the injectors and producers was not considered. It is recommended that these factors be taken into consideration in further research.

NOMENCLATURE

A = Area, ft^2

h = thickness, ft

φ= porosity

k = permeability, mD

μ = viscosity, cp

B = formation volume factor, rb/stb

Sw = Water saturation

V_{DP} = Dykstra-Parsons coefficient

BHP = Bottom-hole pressure, psia

i_w = water injection rate, rb/day

q_o = oil production rate

Subscripts

o = oil

i = initial

n = total number of realizations

h = horizontal

v = vertical

eff = effective

REFERENCES

1. Abbaszadeh M., Ohno K., Okano H. and Morales J., Reservoir Characterization and CO2-EOR Injection Studies in Chicontepec Turbidite Reservoirs, Mexico. Paper IPTC 12637 presented at the International Petroleum Technology Conference held in Kuala Lumpur, Malaysia, 3–5 December 2008.

2. Ahmed T., Reservoir Engineering Handbook, Third Edition, Gulf Professional Publishing, 2006, pp 909 – 916, 927 – 931.

3. Arenas, A. and Dolle N., Smart Waterflooding Tight Fractured Reservoirs Using Inflow Control Valves, paper SPE 84193 presented at the SPE Annual Technical Conference and Exhibition held in Denver, Colorado, 5 - 8 October, 2003.

4. Asadollahi M., 2012. Waterflooding Optimization for Improved Reservoir Management, Ph.D dissertation, Norwegian University of Science and Technology (NTNU), Trondheim, Norway.

5. Asheim H. 1988. Maximization of Water Sweep Efficiency by Controlling Production and Injection Rates. Paper SPE 18365 presented at the SPE European Petroleum Conference, London, UK, October 16-19, 1988.

6. Awejori G.A and Tiab D., Integrated Petrophysical Evaluation of Turbiditic Sands in Niger Delta Basin, MSc. Thesis, Unpublished, AUST, December, 2010.

7. Brouwer, D. R., Jansen, J. D., Van Der Starre, S., van Kruijsdijk, and Berentsen, C. W. J., “Recovery Increase through Waterflooding with Smart Well Technology”, paper SPE

68979 presented at the SPE European Formation Damage Conference held in the Hague, The Netherlands, 21-22 May 2001.

8. Brouwer, D. R. And Jansen, J. D., Dynamic Optimization of Waterflooding with smart Wells Using Optimal Control Theory. Paper SPE 78278-PA, SPEJ 9(4): 391-402, 2004.

9. Cant, D.J., Subsurface facies analysis in Walker and James eds., Facies Models: Response to Sea Level Change: Geological Survey of Canada, 1992.
10.
11. Chang Li, Integration of Facies Models in Reservoir Simulation, Master's Thesis, The University of Texas at Austin, 2010.

12. Coats Engineering, Inc. Sensor Compositional and Black Oil Reservoir Simulation Software, http://coatsengineering.com/sensor_reservoir_simulator.htm, 2013.

13. Craft B.C. and Hawkins M.F., Applied Petroleum Reservoir Engineering. Prentice Hall PTR, Englewood Cliffs, New Jersey, 1991.

14. Craig F.F., The Reservoir Engineering Aspects of Waterflooding. Society of Petroleum Engineers, New York, Dallas, 1971.
15. Ezekwe, J. N., and Filler, S. L.: "Modelling Deepwater Reservoirs," paper SPE 95066 presented at the 2005 SPE Annual Technical Conference and Exhibition held in Dallas, Texas, U.S.A., 9 – 12 October 2005.
16. Handyside D. O., Karaoguz O.K., Deskin R.H. and Mattson G.A. , A Practical Application of Stochastic Modeling Techniques for Turbidite Reservoirs. Paper SPE

24892 presented at the 67th Annual Technical Conference and Exhibition of the Society of Petroleum Engineers held in Washington, DC, October 4-7, 1992.

17. Koederitz L.F., Lecture Notes on Applied Reservoir Simulation, World Scientific, 2004, pp 1-3.

18. Kooli Nader, 2010. Time-Lapse Seismic Monitoring of Waterflooding in Turbidite Reservoirs, Ph.D dissertation, Institute of Petroleum Engineering Heriot-Watt University, Edinburgh, Scotland.

19. Lach Joseph, 2010. IOR for Deepwater Gulf of Mexico: Phase 1, Knowledge Reservoir, Houston, Texas, Dec. 2010

20. Lee, A. S. and Aronofsky, J. S., "A Linear Programming Model for Scheduling Crude Oil Production", Accepted for publication in Journal of Petroleum Technology (July, 1958) vol. 10, No. 7, 51-54.

21. Lyons W.C., Standard Handbook of Petroleum and Natural Gas Engineering, volume 2. 1996.

22. Meshioye O., Mackay E., and Chukuwezi M., Optimization of Waterflooding Using Smart Well Technology. Paper SPE 136996 presented at the 34th Annual SPE International Conference and Exhibition held in Tinapa – Calabar, Nigeria, 31 July–7 August 2010.

23. Nwaozo Jude, 2006, Dynamic Optimization of a Water Flood Reservoir, M Sc. Thesis, University of Oklahoma Graduate College, Norman, Oklahoma, USA.

24. Odai L.A and Ogbe D.O., Building and Ranking of Geostatistical Petroleum Reservoir Models, MSc. Thesis, Unpublished, AUST, December, 2010.

25. Ogali Ikechukwu Oscar, Waterflood Optimization Using Streamline Simulation, MSc. Thesis, Unpublished, AUST, December, 2011.

26. Rose S.C., Buckwalter J.F., and Woodhall R.J.,The Design of Engineering Aspects of Waterflooding. Society of Petroleum Engineers, Richardson, Texas, 1989.

27. Sudaryanto, B. and Yortsos, Y.C. 2001. Optimization of Displacements in Porous Media Using Rate Control. Paper SPE 71509 presented at the SPE Annual Technical Conference and Exhibition, New Orleans, 30 September–3 October. DOI: 10.2118/71509-MS.

28. Tiab, D. (2015), Advanced Petrophysics Lecture Materials, African University of Science and Technology, Abuja, FCT, Nigeria.

29. Wattenbarger R. A., "Maximizing Seasonal Withdrawals from Gas Storage Reservoirs", paper SPE 2406 presented at SPE 44th Annual Fall Meeting in Denver, Colorado, Sept. 28 – Oct 1,1969.

30. Weimer, P. R.M. Slatt, P. Dromgoole, M. Bowman, and A. Leonard, 2000a, Developing and managing turbidite reservoirs: Case histories and experiences- Results from the AAPG/EAGE Research conference: AAPG Bulletin, 84, pg 453-464.

31. Weimer, P. and Slatt, R. M., 1999, Turbidite systems, Part 2: Sub-seismic scale reservoir characteristics, The Leading Edge, May 1999.

APPENDIX

Appendix A

This appendix shows the statistical analysis for petrophysical properties according to the facies observed in the reservoir model. The figures show the histograms and variograms for these properties.

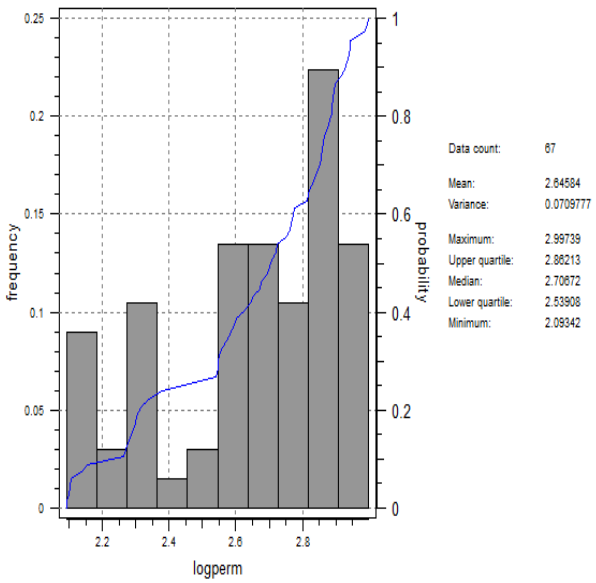

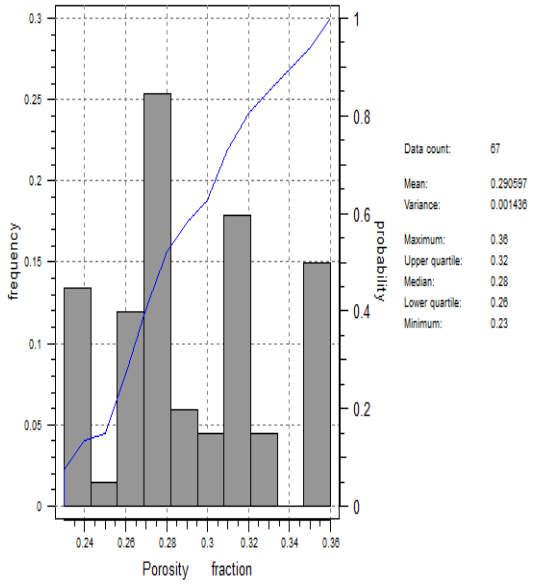

Fig. A.1: Histogram for porosity in facies 1 **Fig. A.2: Permeability Histogram in facies 1**

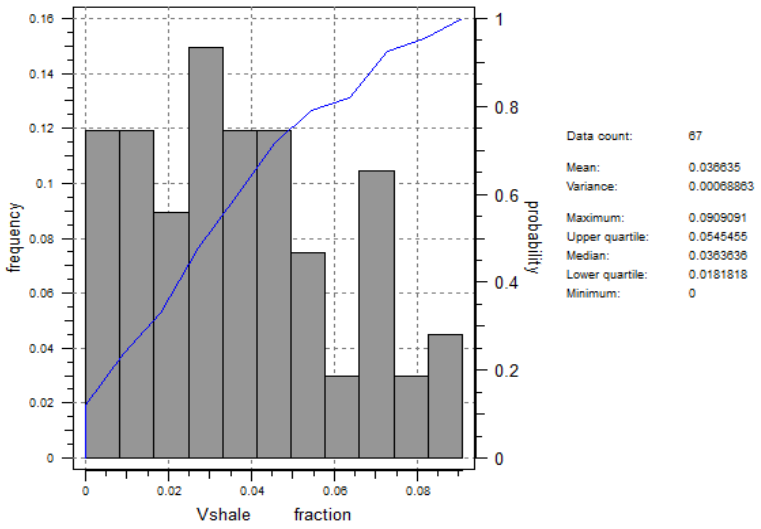

Fig. A.3: Shale volume Histogram for facies 1

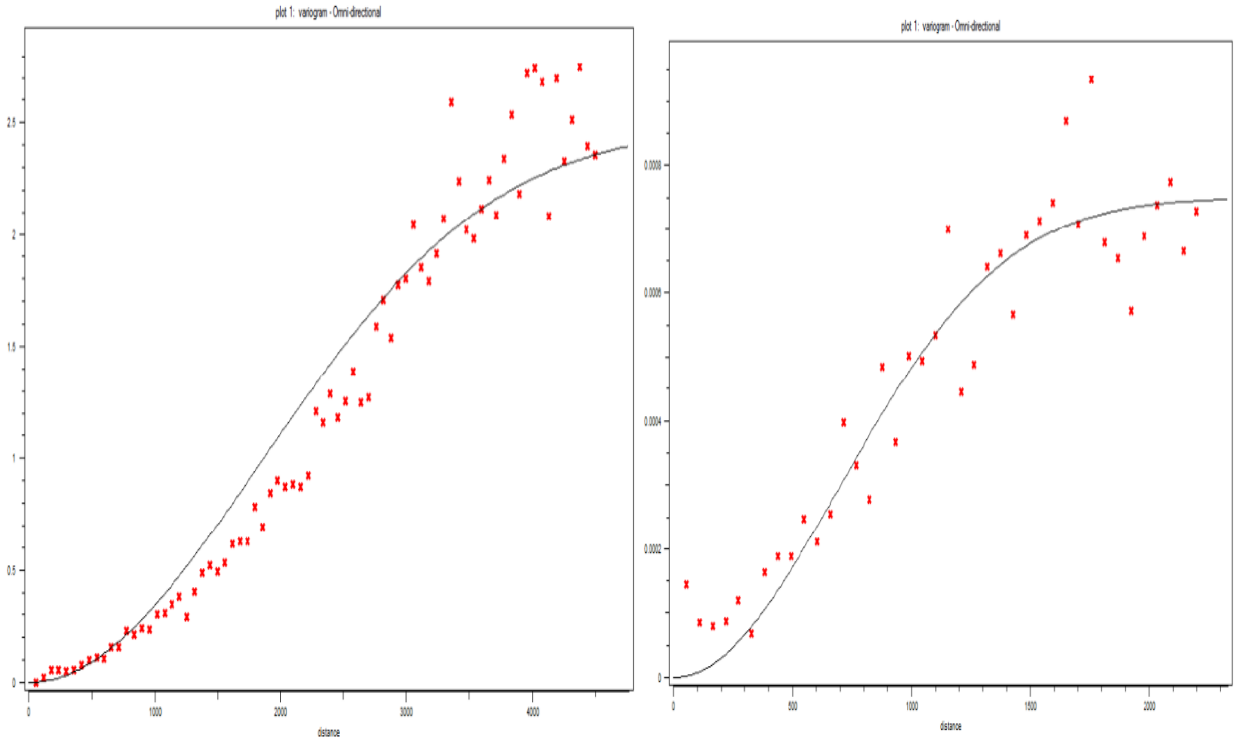

Fig. A.4: Porosity variogram for facies 1 **Fig. A.5: Permeability variogram for facies 1**

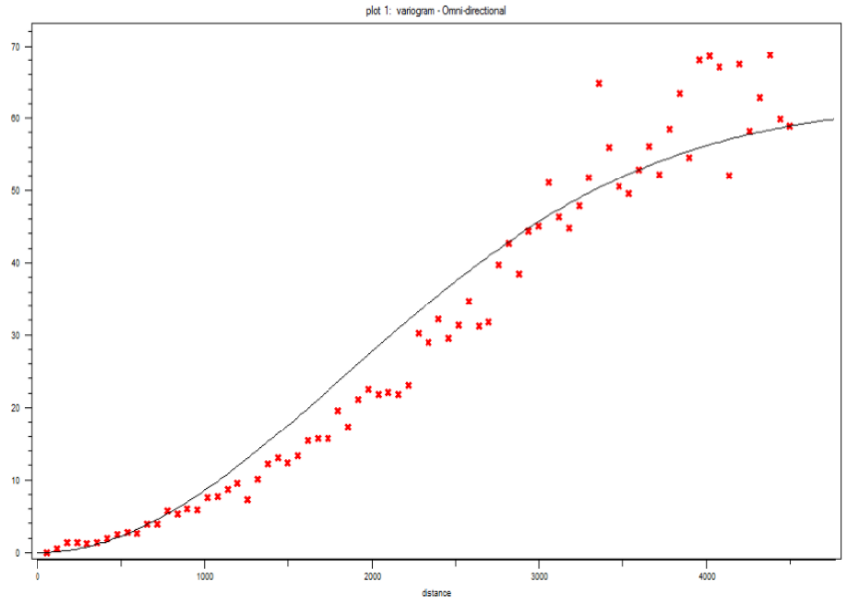

Figure A.6: Variogram for shale volume in facies 1

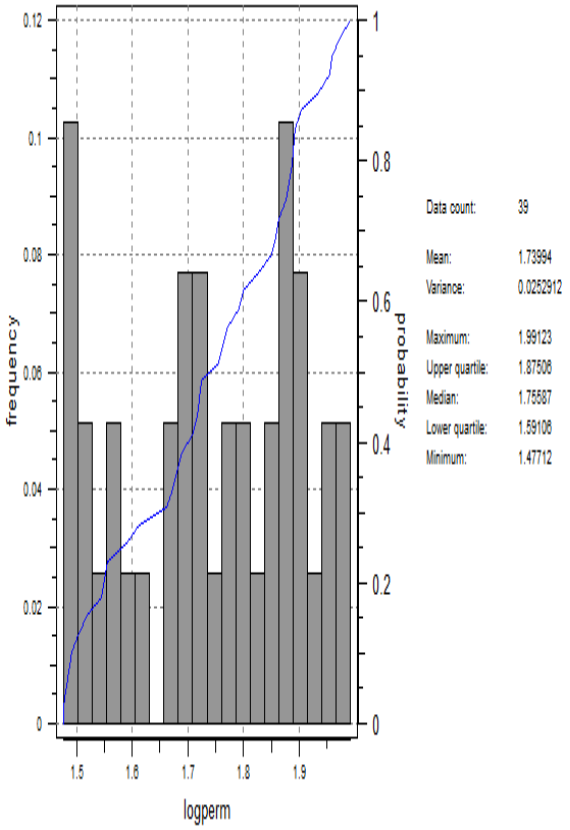

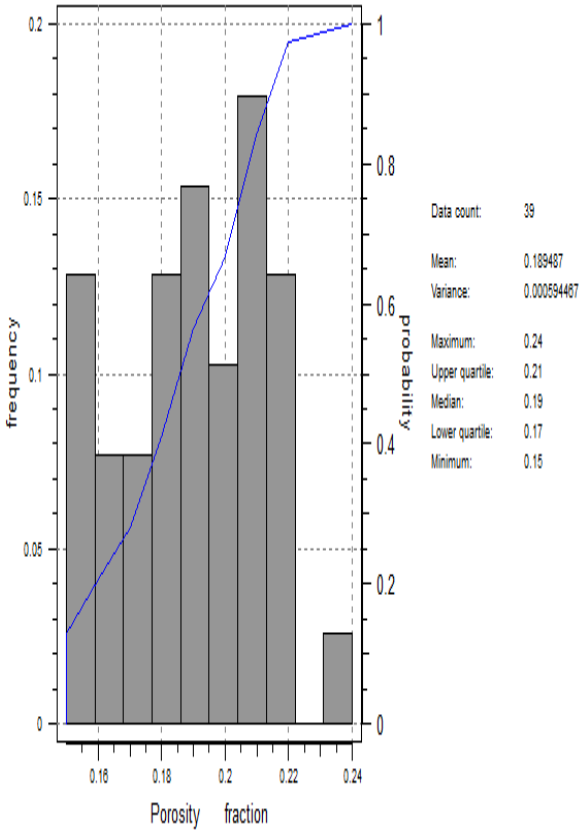

Fig. A.7: Histogram for porosity in facies 2 **Fig. A.8: Permeability Histogram in facies 2**

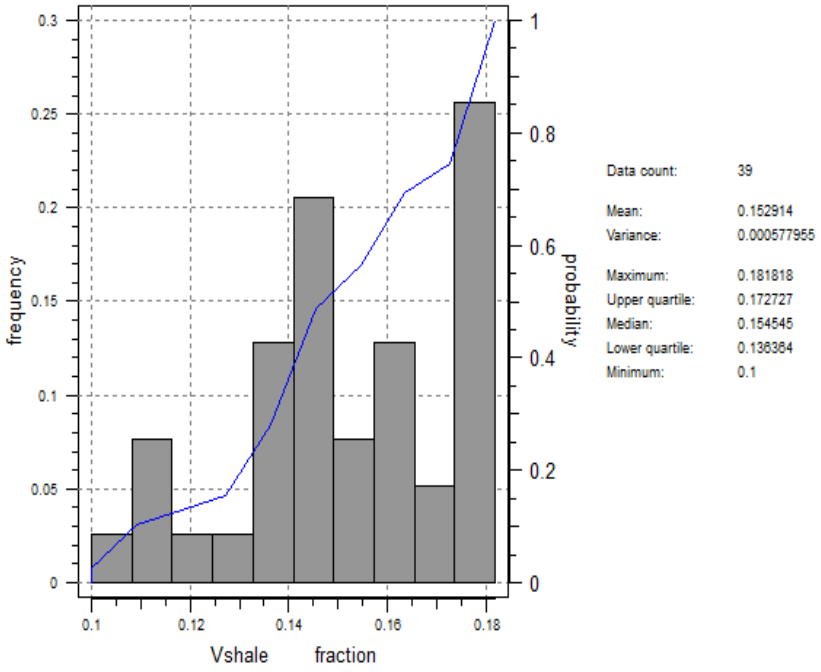

Figure A.9: Histogram for shale volume in facies 2

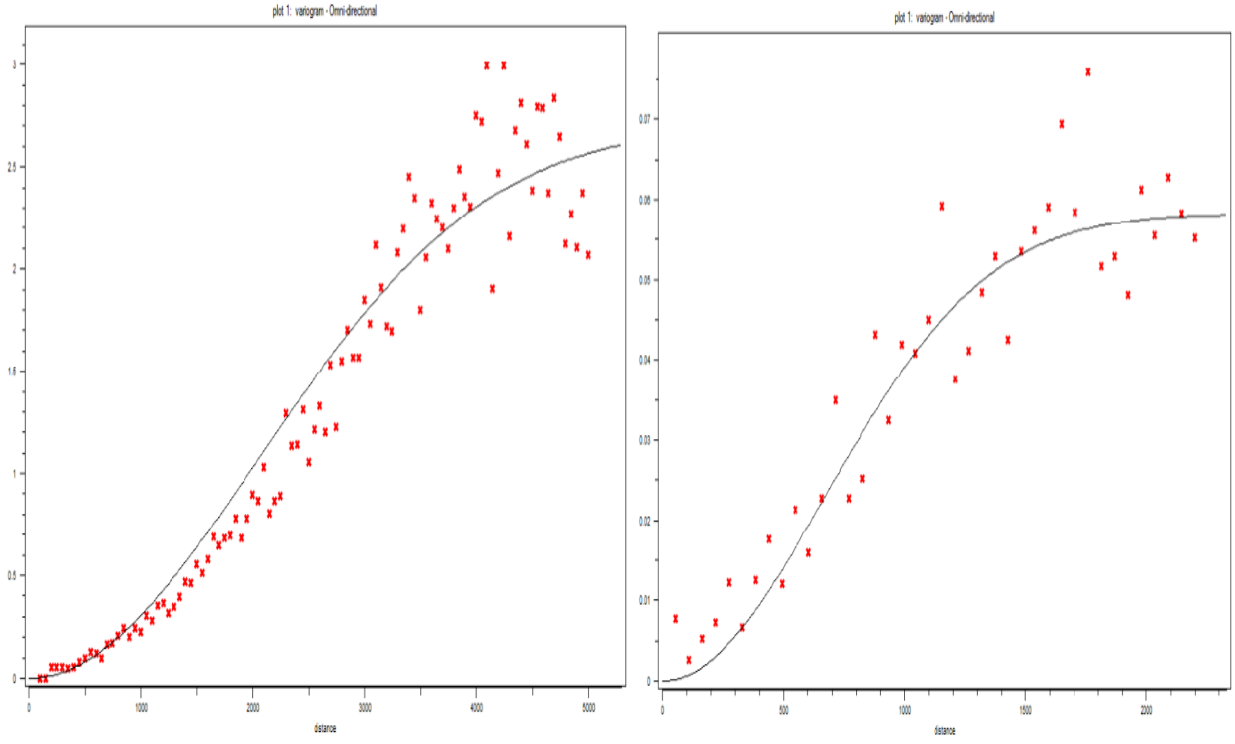

Fig. A.10: Porosity variogram for facies 2 **Fig. A.11: Perm. variogram for facies 2**

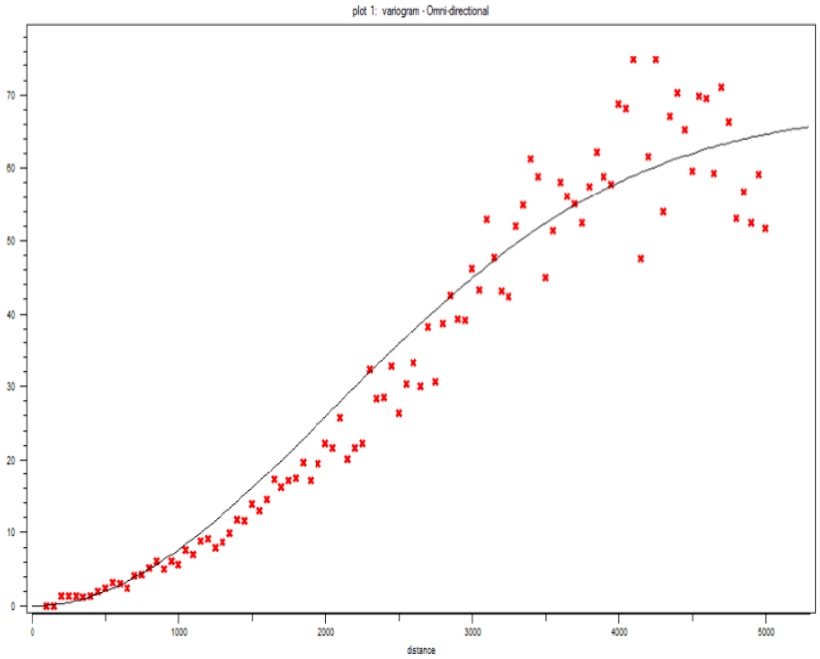

Fig. A.12: Shale volume variogram for facies 2

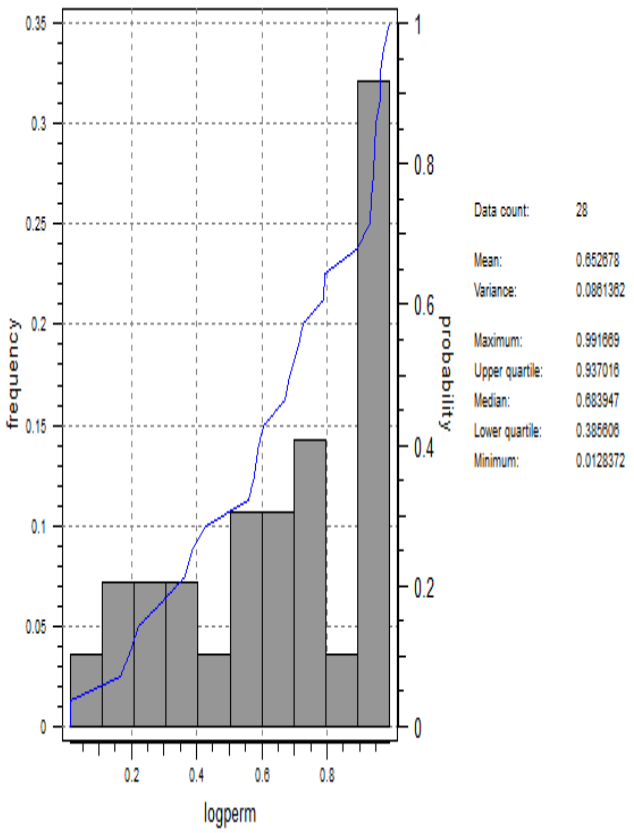

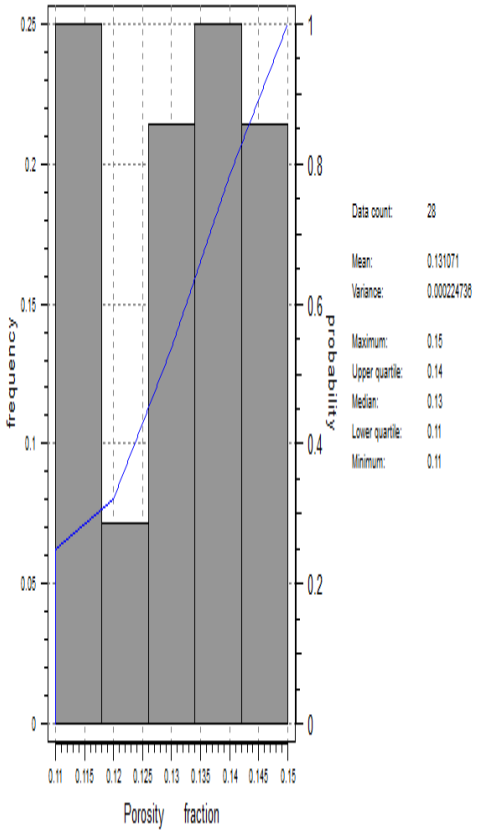

Fig. A.13: Porosity histogram for facies 3

Fig. A.14: Permeability histogram for facies 3

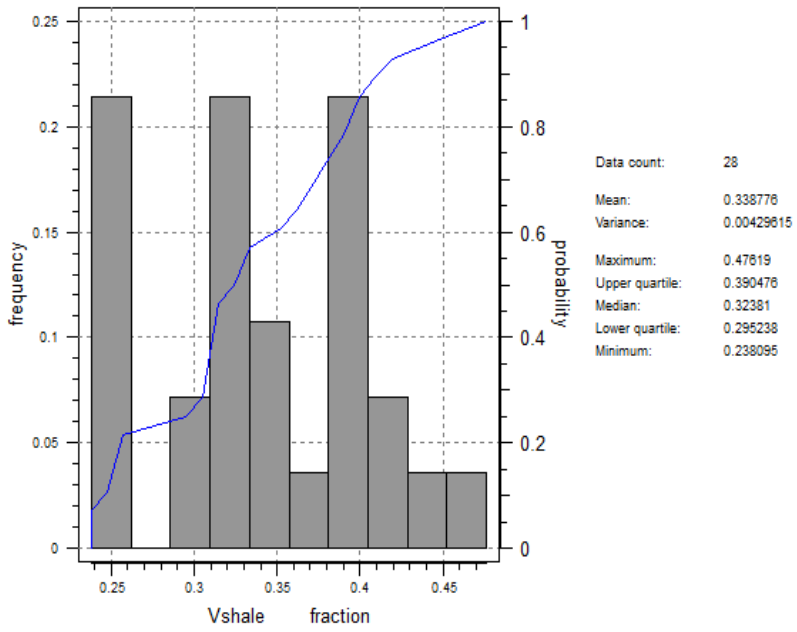

Fig. A.15: Shale volume histogram for facies 3

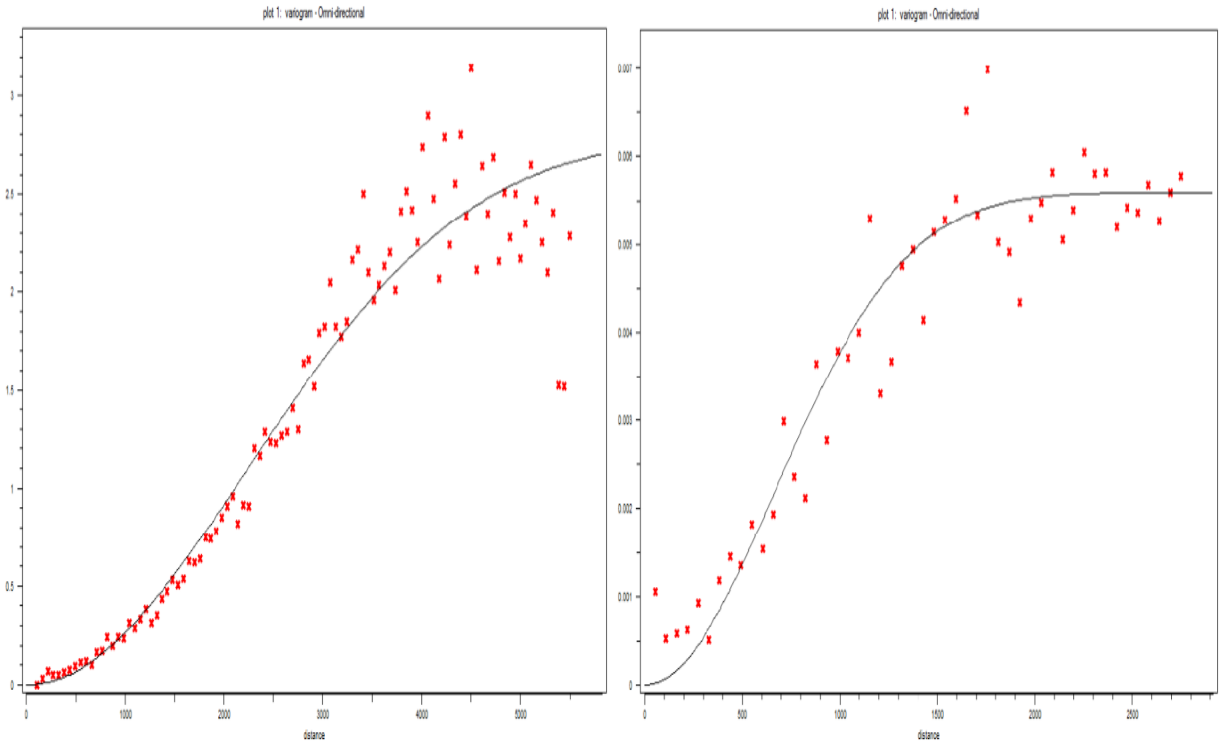

Fig. A.16: Porosity variogram for facies 3 **Fig. A.17: Perm. variogram for facies 3**

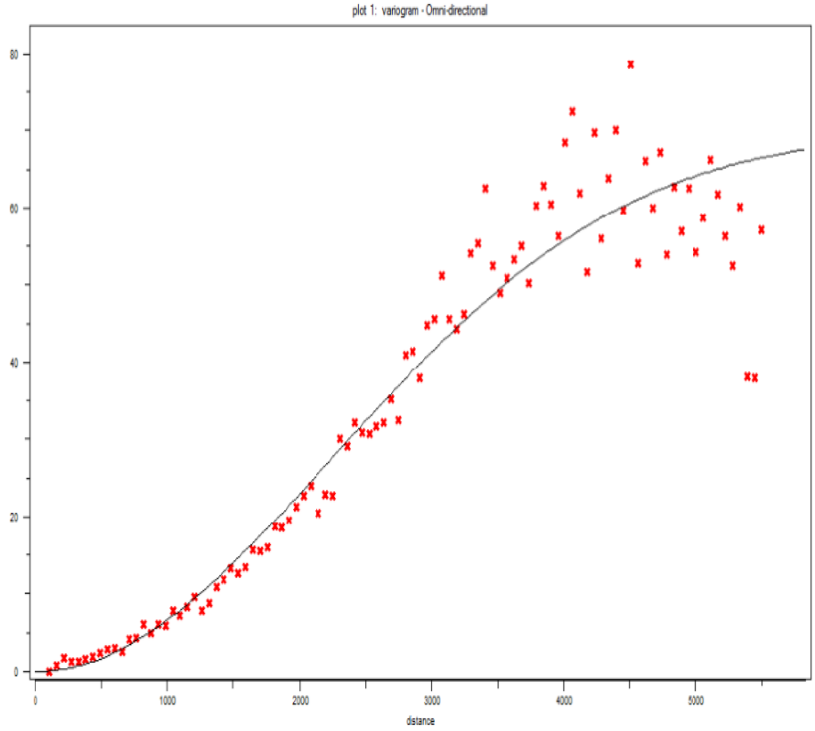

Fig. A.18: Shale volume variogram for facies 3

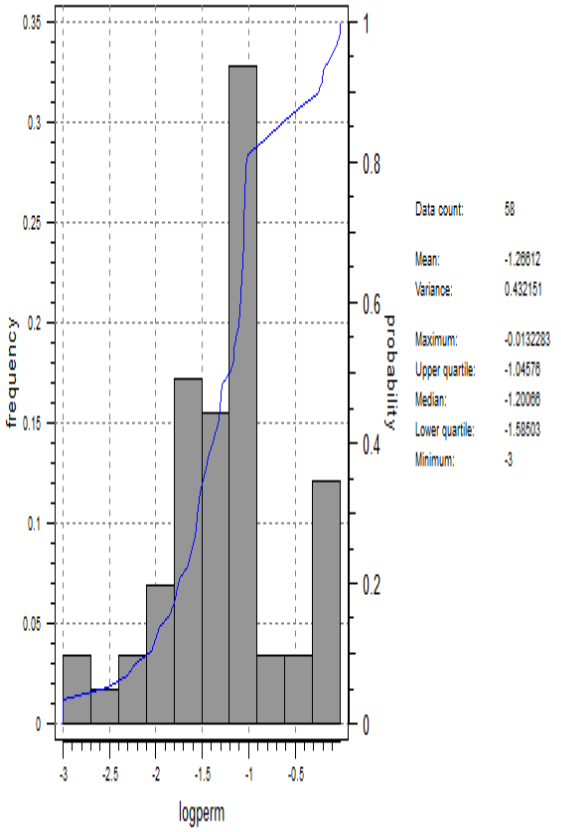

Fig. A.19: Porosity histogram for facies 4

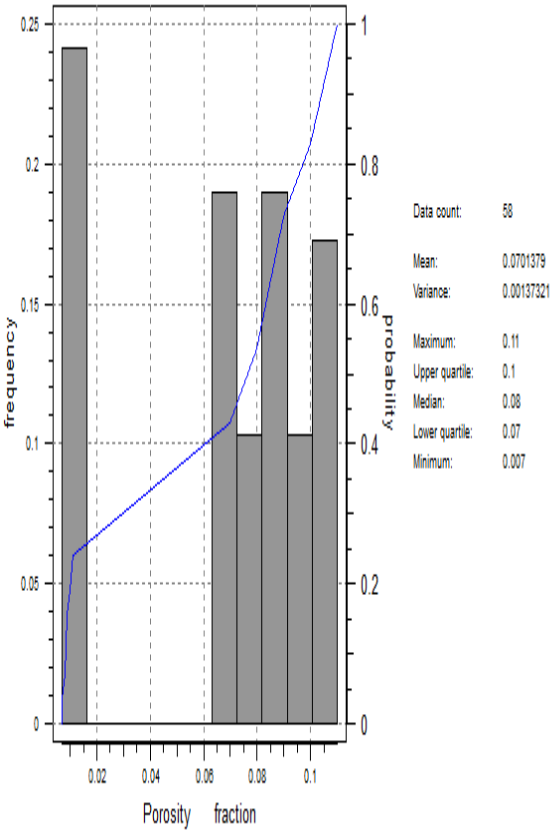

Fig. A.20: Perm. histogram for facies 4

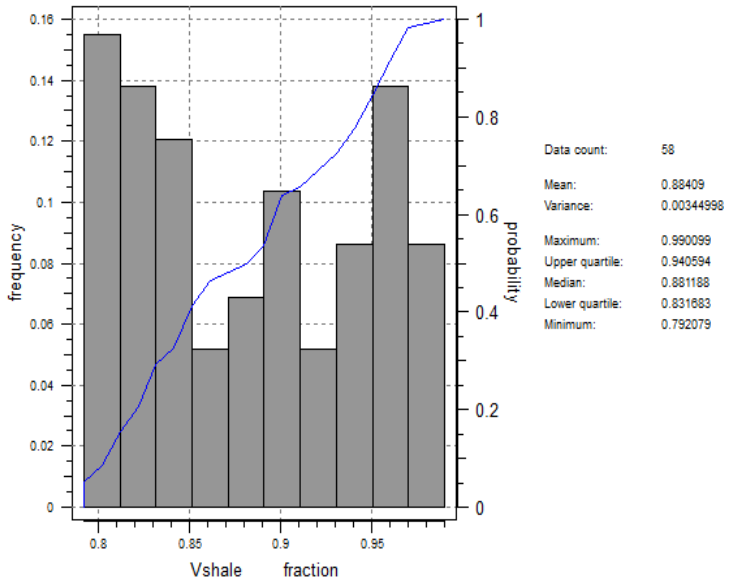

Fig. A.21: Histogram for shale volume in facies 4

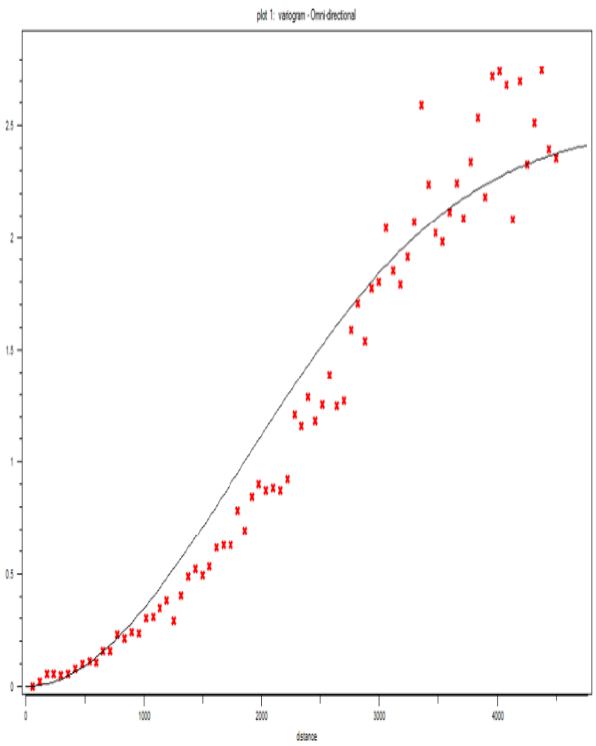

Fig.A.22: Porosity variogram for facies 4

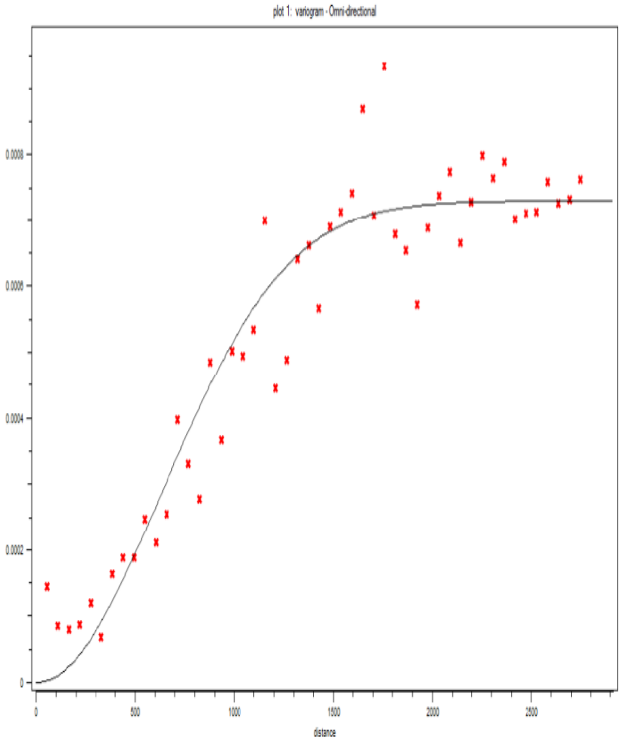

Fig.A.23: Permeability variogram for facies 4

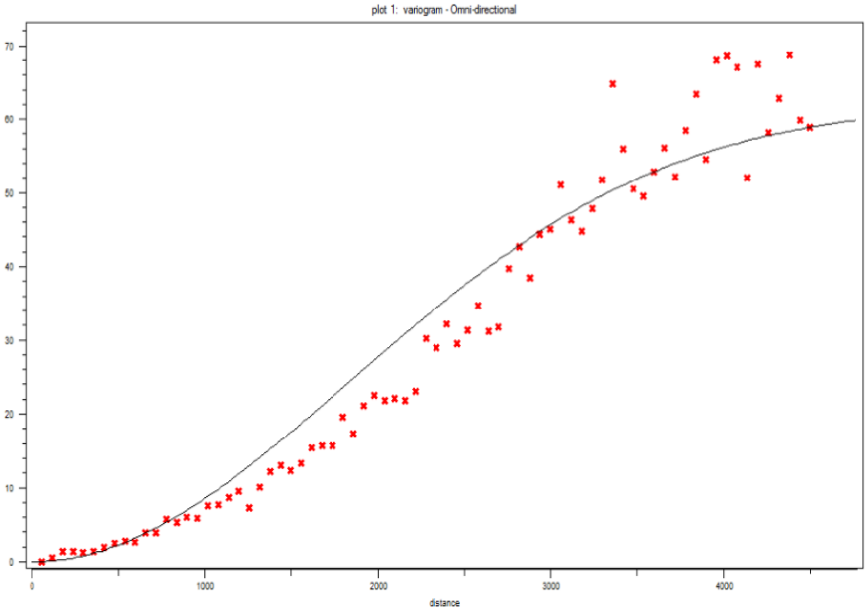

Fig.A.24: Variogram for shale volume in facies 4.

Appendix B

Presented this section of the appendix are the simulation maps for porosity, permeability and shale volume for each facies. The variograms shown in Appendix A1were used in the simulation of these maps.

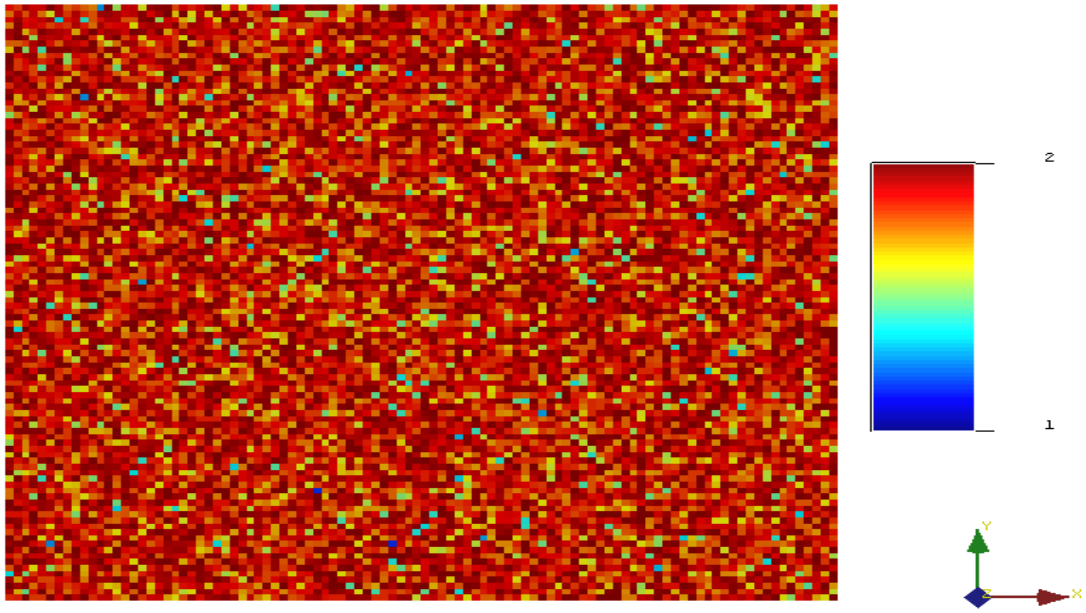

Figure B.1: Simulation map showing facies distribution in layer 2.

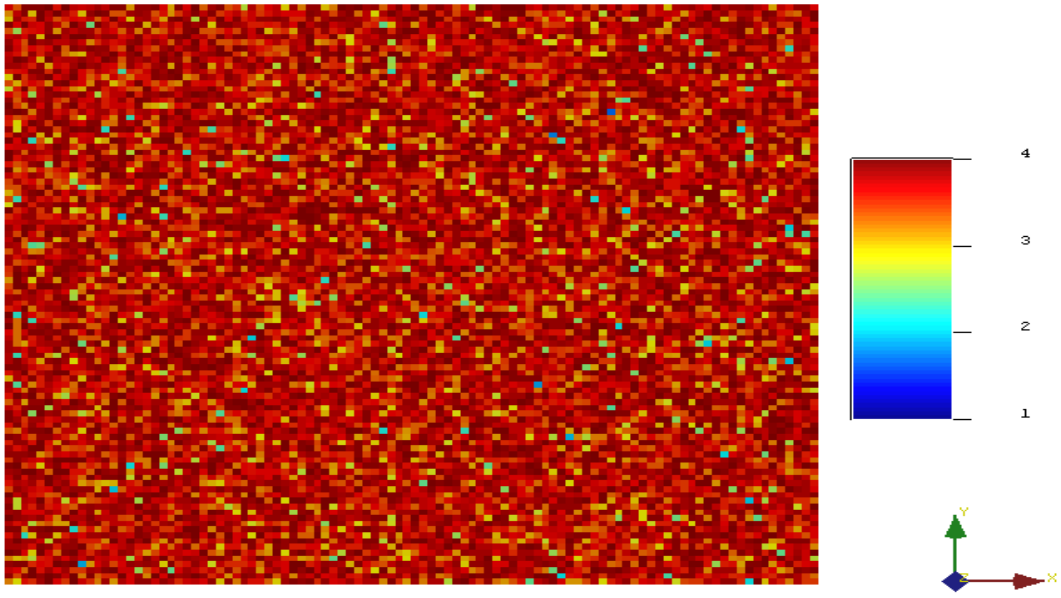

Figure B.2: Simulation map showing facies distribution in layer 5.

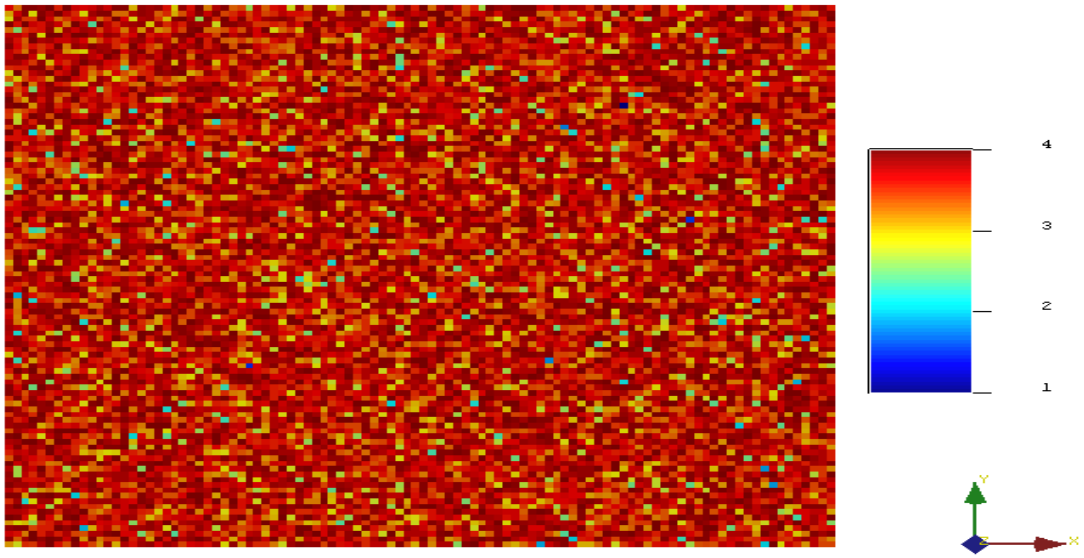

Figure B.3: Simulation map showing facies distribution in layer 10.

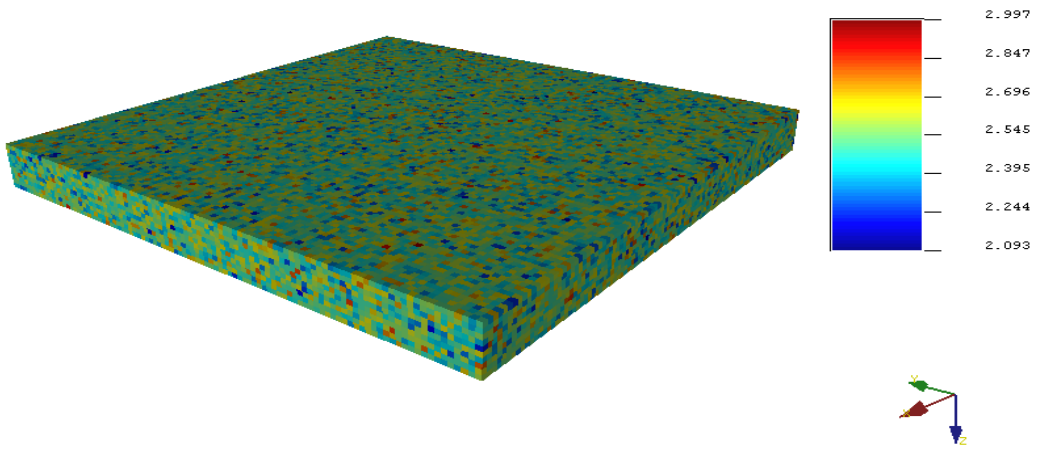

Figure B.4: Simulation map of permeability for facies 1.

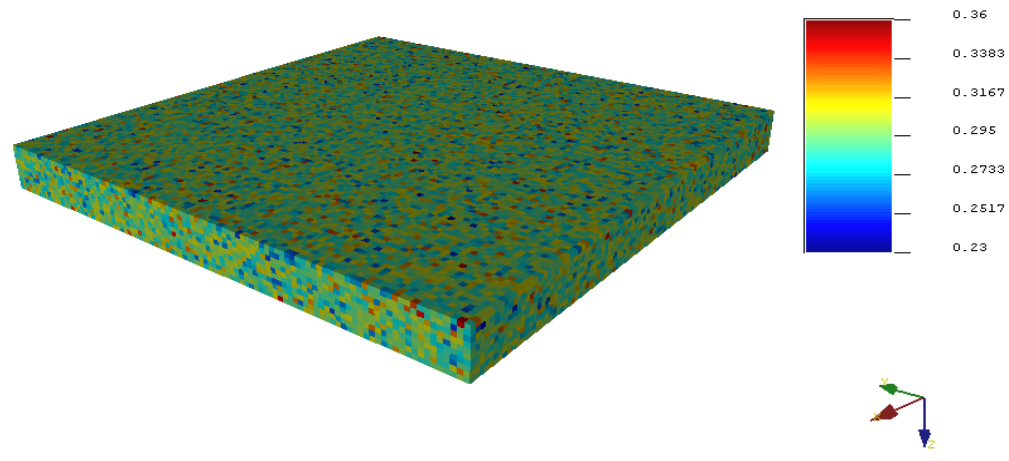

Figure B.5: Simulation map of porosity for facies 1.

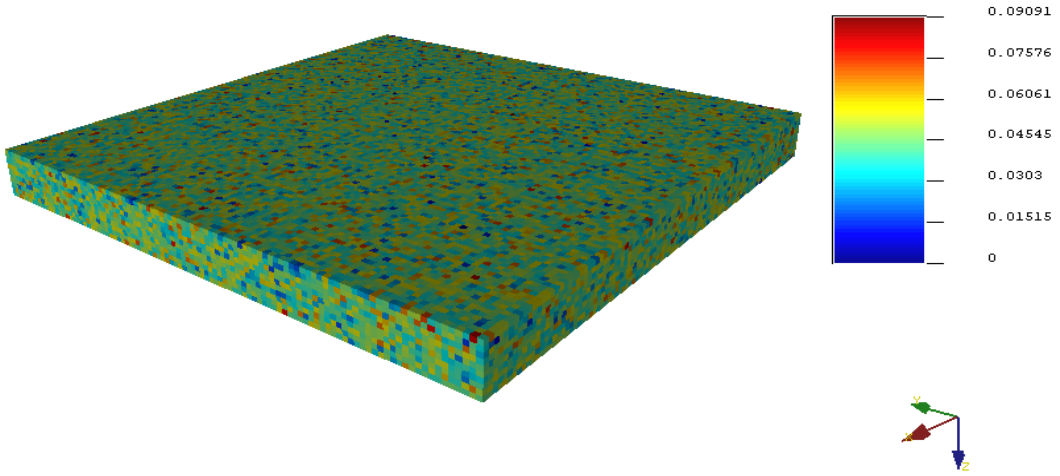

Figure B.6: Simulation map of shale volume for facies 1.

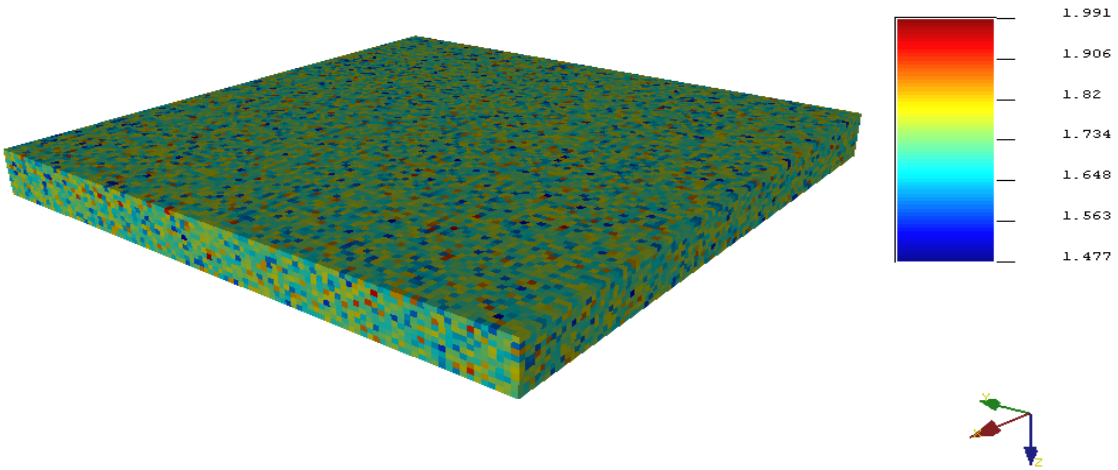

Figure B.7: Simulation map of permeability for facies 2.

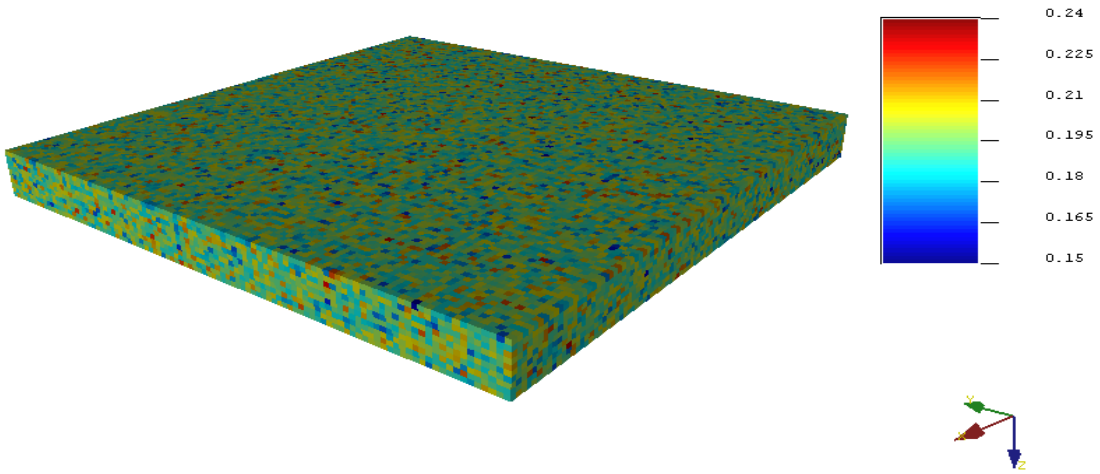

Figure B.8: Simulation map of porosity for facies 2.

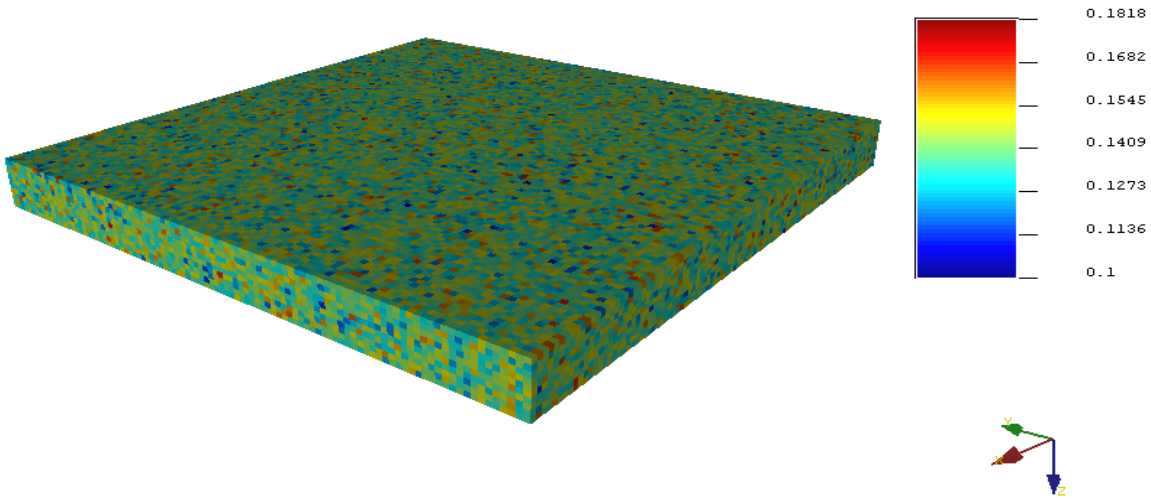

Figure B.9: Simulation map of shale volume for facies 2.

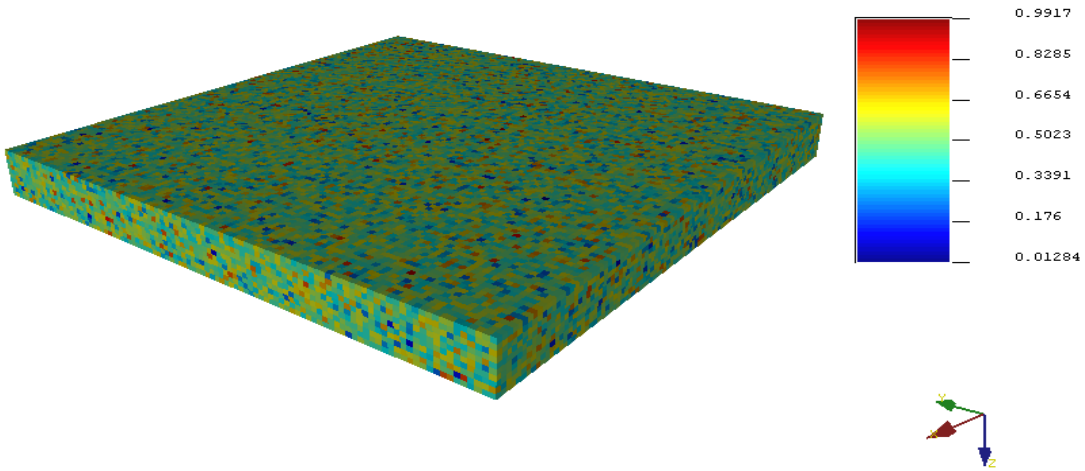

Figure B.10: Simulation map of permeability for facies 3.

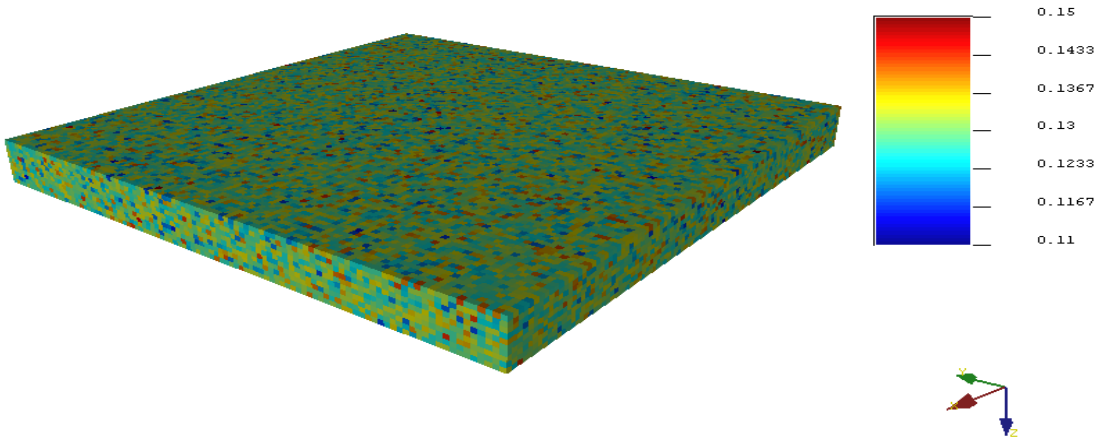

Figure B.11: Simulation map of porosity for facies 3.

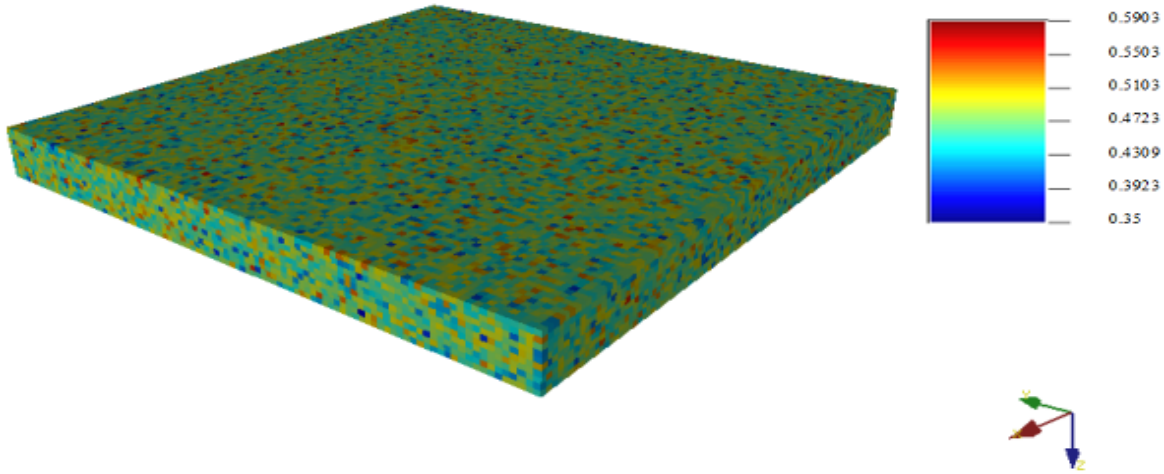

Figure B.12: Simulation map of shale volume across facies 3.

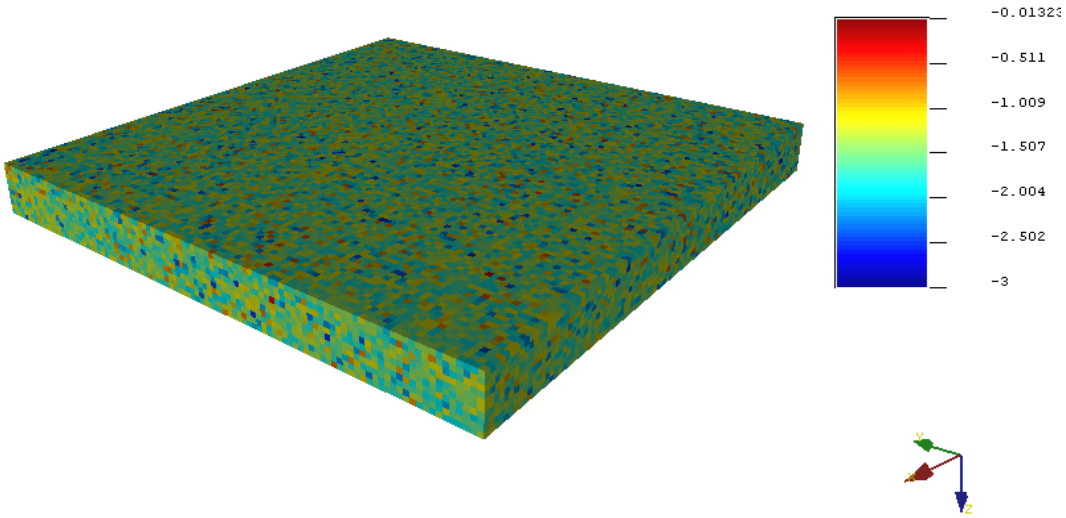

Figure B.13: Simulation map of permeability for facies 4.

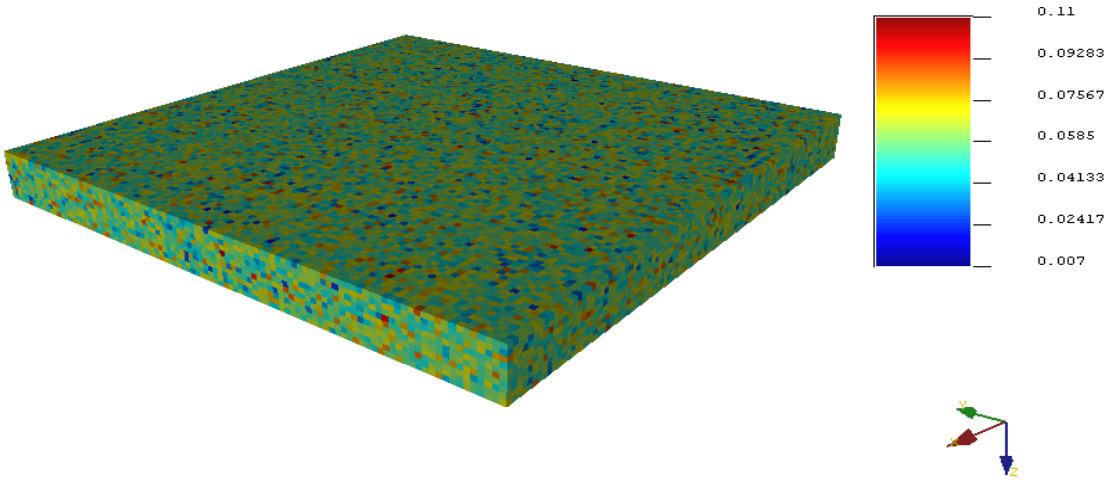

Figure B.14: Simulation map of porosity for facies 4.

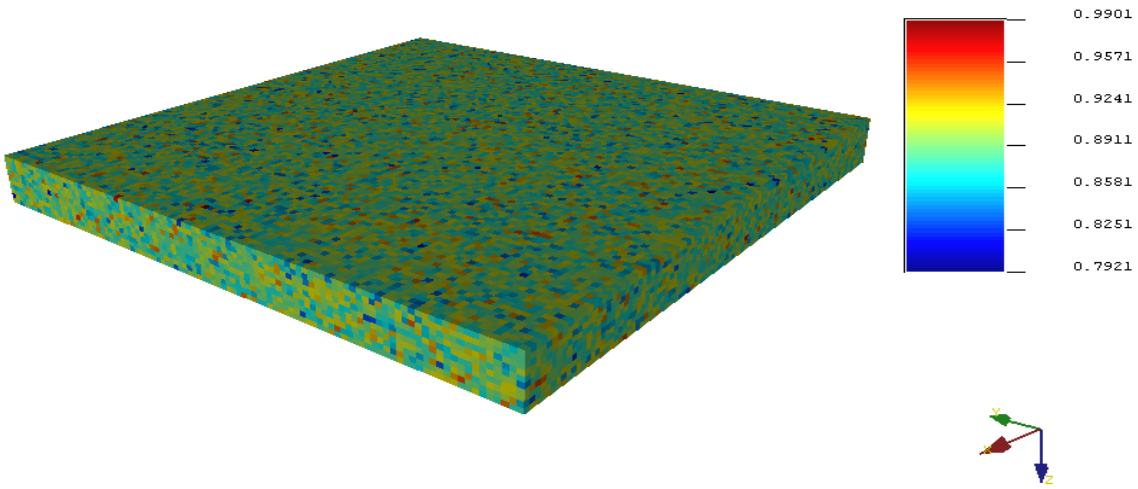

Figure B.15: Simulation map of shale volume across facies 4.

Appendix C

This appendix presents the derivation of the equation used in estimating horizontal and vertical permeabilities(Equations 3.9 through 3.12).

Proof:

It is known that average permeability k_{avg} is given as:

$$k_{avg} = \sqrt[3]{k_X . k_Y . k_Z} \quad \text{---------- C.1}$$

where k_x,k_y and k_z are the permeability in the x, y and z directions respectively.

Therefore,

$$k_{avg}{}^3 = k_X . k_Y . k_Z \quad \text{---------- C.2}$$

But, horizontal permeability, k_H is given as:

$$k_H = \sqrt{k_X . k_Y} \quad \text{---------- C.3}$$

Therefore,

$$k_H{}^2 = k_X . k_Y \quad \text{---------- C.4}$$

Equation C.2 therefore becomes:

$$k_{avg}{}^3 = k_H{}^2 . k_Z \quad \text{---------- C.5}$$

Using a range of kV/kH ratios, for instance 0.001, 0.01, 0.1 and 0.6, it is derived that

$$k_Z = k_H . x \quad \text{---------- C.6}$$

where $k_V = k_Z$ and x = 0.001, 0.01, 0.1 or 0.6.

Combining equations C.5 and C.6, we have that:

$$k_{avg}{}^3 = k_H{}^2 . k_H . x \quad \text{---------- C.7}$$

This means that:

$$k_{avg}{}^{3} = k_{H}{}^{3}.x \quad \text{---------- C.8}$$

Therefore,

$$k_{avg} = k_{H}.\sqrt[3]{x} \quad \text{---------- C.9}$$